ARMY RESEARCH LABORATORY

Through-the-Wall Small Weapon Detection Based on Polarimetric Radar Techniques

by Traian Dogaru and Calvin Le

ARL-TR-5041 **December 2009**

NOTICES

Disclaimers

The findings in this report are not to be construed as an official Department of the Army position unless so designated by other authorized documents.

Citation of manufacturer's or trade names does not constitute an official endorsement or approval of the use thereof.

Destroy this report when it is no longer needed. Do not return it to the originator.

Army Research Laboratory
Adelphi, MD 20783-1197

ARL-TR-5041 **December 2009**

Through-the-Wall Small Weapon Detection Based on Polarimetric Radar Techniques

Traian Dogaru and Calvin Le
Sensors and Electron Devices Directorate, ARL

REPORT DOCUMENTATION PAGE	Form Approved OMB No. 0704-0188

1. REPORT DATE *(DD-MM-YYYY)*	2. REPORT TYPE	3. DATES COVERED (From - To)
December 2009	Final	2009

4. TITLE AND SUBTITLE	5a. CONTRACT NUMBER
Through-the-Wall Small Weapon Detection Based on Polarimetric Radar Techniques	5b. GRANT NUMBER
	5c. PROGRAM ELEMENT NUMBER
6. AUTHOR(S)	5d. PROJECT NUMBER
Traian Dogaru and Calvin Le	5e. TASK NUMBER
	5f. WORK UNIT NUMBER
7. PERFORMING ORGANIZATION NAME(S) AND ADDRESS(ES)	**8. PERFORMING ORGANIZATION REPORT NUMBER**
U.S. Army Research Laboratory ATTN: RDRL-SER-U 2800 Powder Mill Road Adelphi, MD 20783-1197	ARL-TR-5041
9. SPONSORING/MONITORING AGENCY NAME(S) AND ADDRESS(ES)	**10. SPONSOR/MONITOR'S ACRONYM(S)**
	11. SPONSOR/MONITOR'S REPORT NUMBER(S)

12. DISTRIBUTION/AVAILABILITY STATEMENT

Approved for public release; distribution unlimited.

13. SUPPLEMENTARY NOTES

14. ABSTRACT

In this report, we investigate techniques for small weapon detection in the context of sensing-through-walls radar sensors. Our approach exploits the radar wave polarization in order to discriminate between a human carrying a weapon and an unarmed human. We first develop a polarization optimization procedure for a rifle-like target, but demonstrate that this technique does not perform as expected in the presence of a human. Next, we introduce a more robust discrimination procedure based on the ratio of the cross- to co-polarization radar signature. We show that this technique produces a measurable enhancement (of at least 8 dB) when the human carries a weapon versus the case of an unarmed human. We support this idea with numerical examples that include radar cross section evaluations, synthetic aperture radar images of humans in rooms of various complexities, and the Doppler spectrum of a moving human.

15. SUBJECT TERMS

Radar, concealed weapons

16. SECURITY CLASSIFICATION OF:			17. LIMITATION OF ABSTRACT	18. NUMBER OF PAGES	19a. NAME OF RESPONSIBLE PERSON
a. REPORT	b. ABSTRACT	c. THIS PAGE			Traian Dogaru
Unclassified	Unclassified	Unclassified	UU	46	19b. TELEPHONE NUMBER **(*Include area code*)** (301) 394-1482

Standard Form 298 (Rev. 8/98)
Prescribed by ANSI Std. Z39.18

Contents

List of Figures

List of Tables

Acknowledgments

This study was partially funded by the Communications-Electronics Research Development and Engineering Center (CERDEC), Intelligence and Information Warfare Directorate (I2WD) at Ft. Monmouth, NJ. We would like to acknowledge our U.S. Army Research Laboratory (ARL) colleagues, Kenneth Ranney and Anders Sullivan, for their advice regarding various parts of this report, and Getachew Kirose for his contribution to the computer modeling of the moving human.

.

1. Introduction

The U.S. Army Research Laboratory (ARL) has been recently involved in several programs related to sensing-through-the-wall (STTW) radar technology. A significant part of our efforts consisted of computer models of various scenarios relevant to this technology, with the purpose of predicting performance and analyzing the radar system parameter trade-off. Some of our previous studies included human radar signature analysis (*1*), modeling of radar imaging systems for building mapping (*2*), validating radar signature computational codes for STTW applications (*3, 4*), and Doppler radar signature analysis of a moving human (*5*). This report tackles another problem of great interest in the context of radar sensors for concealed environments—through-the-wall detection of small weapons carried by humans.

Detecting concealed small weapons carried by people has received significant interest from law enforcement agencies as well as the military, most frequently for application in controlling checkpoints (in airports, border crossing, public spaces, etc.). Imaging systems for concealed weapons based on radar or other sensor technologies have been recently developed and tested. Most of the existing electromagnetic (EM) sensors suitable for this application operate at very high frequencies, usually in the millimeter or terahertz frequency bands and produce high-resolution images (*6–8*). Although these EM waves can penetrate through clothing (textile materials), they have very poor penetration properties through many common construction materials (such as brick or concrete). Most through-the-wall radars must operate at much lower frequencies, usually below 4 GHz (*9*), in order to "see" targets behind walls. However, at those low frequencies, the image resolution is degraded, so small weapons carried by humans may be difficult to detect directly in the image domain.

In this study, we propose an approach based on polarimetric radar techniques for through-the-wall detection of certain weapons, such as rifles or rocket propelled grenade (RPG) launchers. In order to make these techniques effective, the targets must exhibit a large shape factor (the target must extend in one dimension much more than in the other two) and be made mostly of metal. The radar signature of these targets is very sensitive to wave polarization (more exactly, to the orientation of the electric field vector in the plane perpendicular to the direction of propagation) and we try to exploit that in the STTW imaging radar system. An additional requirement for our detection problem is being able to find a weapon placed close to a human body—in other words, we want to be able to discriminate a human carrying a weapon from one without a weapon. This presents an additional challenge to the system, since generally the human signature is significantly larger than that of a rifle or RPG. We would also like to be able to detect multiple weapon carriers within a scene, with the targets placed in arbitrary orientations.

In section 2, we introduce an approach based on optimizing the radar polarization for maximum target signature. We demonstrate this idea on an isolated rifle placed in free space. At the same time, we show that this technique breaks down in the more complicated scenario where the rifle is carried by a human. Section 3 examines a more robust approach, based on comparing the cross- and co-polarization responses from targets. This method has a much better potential to allow discrimination between humans with and without weapons. We also show how this technique can be applied to various STTW scenarios (imaging or Doppler radar), for various targets in arbitrary orientations. All the numerical examples presented in this study are based on computer simulations. We draw conclusions in section 4.

2. Polarization Dependent Optimization of the Radar Signature

In this section, we investigate a procedure that optimizes the radar polarization in order to maximize the weapon signature. We consider the case of an AK-47 rifle. It is well known that an object with a rod-like geometry has the largest radar response when the electric field vector of the radar wave is aligned with the long axis of the target. In the case when the target orientation is unknown, the fully polarimetric scattering matrix (based on two orthogonal polarizations, usually vertical and horizontal) contains all the information necessary to find the optimal orientation of the polarization (or electric field) vector. Thus, by performing the required transformation on the scattering matrix (which consists of a rotation of the polarization vector in a plane perpendicular to the direction of propagation), we can enhance the response of a target with certain geometric characteristics that are polarization-sensitive.

Consider a metallic rod such as that shown in figure 1. The rod is placed in a plane perpendicular to the direction of propagation and tilted at angle α. We also assume that the radar is in the far-field and looks at 0° elevation (the propagation vector is in the *x*-*y* plane). The plane perpendicular to the propagation direction is defined by two orthogonal unit vectors, $\mathbf{u_v}$ (vertical) and $\mathbf{u_h}$ (horizontal). For instance, if the propagation direction is aligned with the *x*-axis, then $\mathbf{u_h}$ is along the *y*-axis and $\mathbf{u_v}$ along the *z*-axis. For a plane wave, the electric field vector **E** is contained in the plane defined by $\mathbf{u_v}$ and $\mathbf{u_h}$, with components E_v and E_h.

$$\mathbf{E} = E_v \mathbf{u}_\mathbf{v} + E_h \mathbf{u}_\mathbf{h} = \begin{bmatrix} E_v \\ E_h \end{bmatrix} \tag{1}$$

where

$$\mathbf{u}_\mathbf{v} = \begin{bmatrix} 1 \\ 0 \end{bmatrix} \text{ and } \mathbf{u}_h = \begin{bmatrix} 0 \\ 1 \end{bmatrix} \tag{2}$$

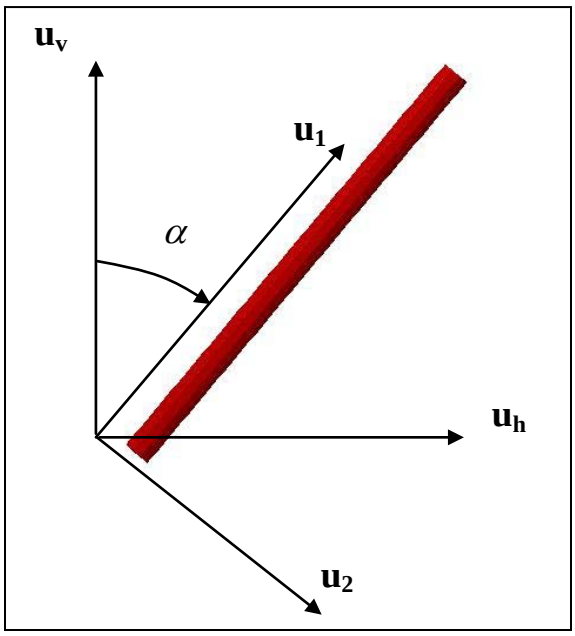

Figure 1. A simple cylindrical rod tilted at angle α with respect to vertical, showing the electric field unit vectors in two different coordinate systems.

In the most general case, E_v and E_h are complex numbers (elliptical polarization). However, for linear polarization, the E_v to E_h ratio is real. For this geometry, the scattering matrix **S** relates the incident and scattered electric field vectors $\mathbf{E^i}$ and $\mathbf{E^s}$ by the following equation:

$$\mathbf{E^s} = \frac{e^{-jk_0 r}}{r}\mathbf{S}\mathbf{E^i} \tag{3}$$

where

$$\mathbf{S} = \begin{bmatrix} S_{vv} & S_{vh} \\ S_{hv} & S_{hh} \end{bmatrix} \tag{4}$$

It can be shown that the target's backscatter signature is maximized when the electric field vector (both at the transmitter and at the receiver) is aligned with the eigenvector corresponding to the maximum eigenvalue (in magnitude) of the matrix **S*S** (*11*, *12*). For a target with a rod-like geometry, we expect the polarization direction that maximizes the signature to coincide with its long axis, which forms an angle α with the vertical direction (figure 1). We also expect the components of the corresponding eigenvector to be real (linear polarization). Assuming that **S*S** has distinct eigenvalues, let $\mathbf{u_1}$ and $\mathbf{u_2}$ the two normalized eigenvectors ($\mathbf{u_1}$ corresponding to the maximum eigenvalue). Then, we can write

$$\mathbf{u_1} = \cos\alpha\,\mathbf{u_v} + \sin\alpha\,\mathbf{u_h} = \begin{bmatrix} \cos\alpha \\ \sin\alpha \end{bmatrix} \tag{5}$$

$$\mathbf{u}_2 = -\sin\alpha\,\mathbf{u}_\mathbf{v} + \cos\alpha\,\mathbf{u}_\mathbf{h} = \begin{bmatrix} -\sin\alpha \\ \cos\alpha \end{bmatrix} \tag{6}$$

The unit vectors $\mathbf{u_1}$ and $\mathbf{u_2}$ form a new orthogonal basis in the **E** vector plane that is obtained from the original $\mathbf{u_v}$ and $\mathbf{u_h}$ basis by a rotation of angle α. The transformation (rotation) matrix is

$$\mathbf{R} = \begin{bmatrix} \cos\alpha & -\sin\alpha \\ \sin\alpha & \cos\alpha \end{bmatrix} \tag{7}$$

Under this transformation, the scattering matrix becomes

$$\mathbf{S}^{opt} = \mathbf{R}^{*T}\mathbf{S}\mathbf{R} = \begin{bmatrix} S_{11}^{opt} & S_{12}^{opt} \\ S_{21}^{opt} & S_{22}^{opt} \end{bmatrix} \tag{8}$$

It can be shown (*12*) that the new scattering matrix is diagonal and that S_{11}^{opt} is the square root of the maximum eigenvalue of matrix **S*S**. This element can be used in further processing of the radar data, yielding the maximum radar response of the target within the entire polarization space. Clearly, in order to compute S_{11}^{opt}, we need to first obtain all four elements of the polarimetric matrix (through either modeling or measurements).

As a first verification of this approach, we apply it to a cylindrical metallic rod of 1 m length and 6 cm diameter (figure 2a). In particular, we look at the following problem: given the scattering data from the rod placed in an unknown orientation, can we estimate the tilt angle (in the plane perpendicular to the radar line of sight)? Our approach consists of computing the fully polarimetric radar response of the rod at various angles between 0° and 90° (measured from vertical) and trying to infer the tilt angle α from the two components of the $\mathbf{u_1}$ vector by the procedure outlined above. All our simulations in this report use the AFDTD electromagnetic modeling code, which was entirely developed at ARL for radar signature calculations. This code is based on the Finite-Difference Time-Domain (FDTD) method (a comprehensive introduction of this technique can be found in reference 10). The simulations are run in a frequency band extending from 0.5 to 2.5 GHz. The estimated angle α should theoretically be independent of frequency. However, in order to improve the reliability of this procedure, we average the estimated angle over the entire frequency band. The tilt angle estimation results are shown in figure 2b, together with the real tilt angles. In this case, the estimation procedure works perfectly.

In the next step, we apply the same procedure to simulation data obtained on an AK-47 rifle placed in free space. Representations of the AK-47 computer meshes are shown in figure 3, where the metallic parts are painted brown and the wooden parts are painted yellow (the wooden parts are shown as transparent in order to evidence the internal structure including the continuous metallic barrel). Unless specified otherwise, the mesh has a resolution (cell size) of 2 mm. The wood dielectric constant is $\varepsilon_r = 2$. The simulations are run in the same frequency band as in the previous example. The estimated tilt angles (together with the real tilt angles) are shown in

figure 4. We notice that in this case the procedure produces a small error (generally less than 5°), but the estimate is still fairly accurate. We can probably attribute the error to the more complex shape of the AK-47 (especially the bullet magazine, which is oriented almost perpendicularly to the barrel).

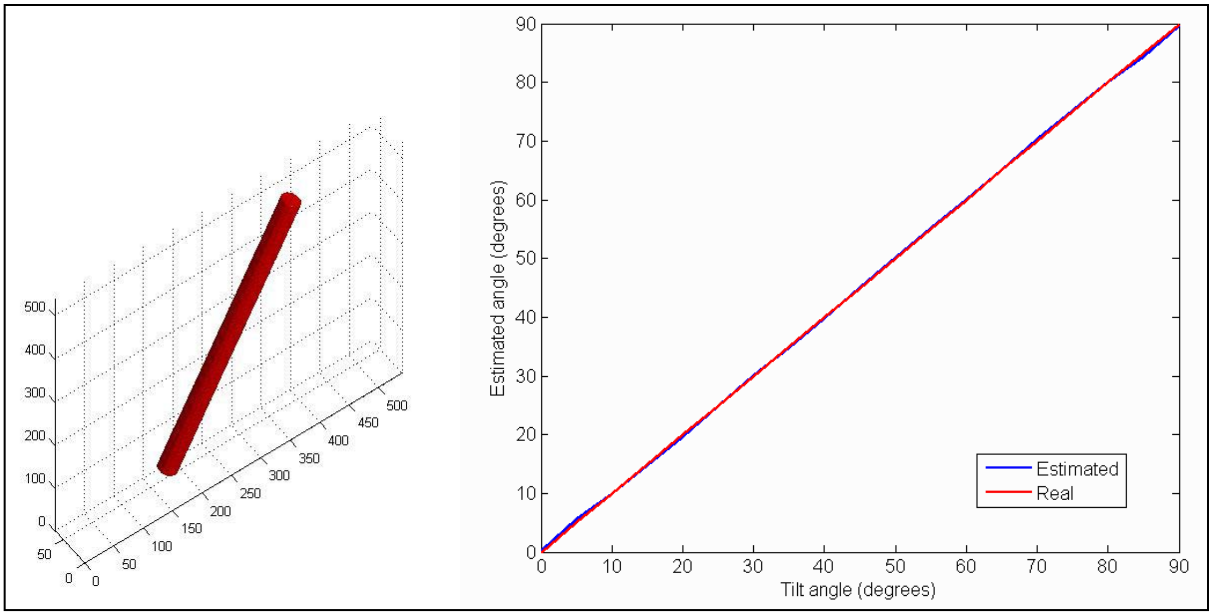

Figure 2. Estimating the tilt angle of a cylindrical metallic rod of 1 m length and 6 cm diameter. (a) View of the FDTD mesh with 2-mm resolution and (b) the tilt angle estimation results.

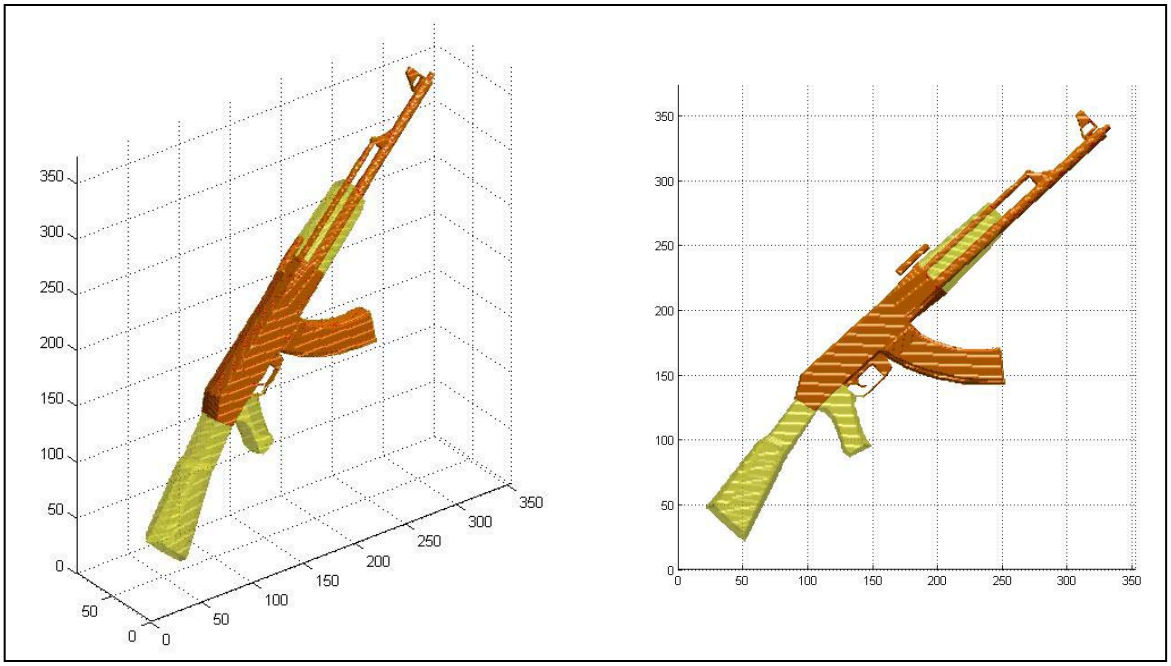

Figure 3. Different views of the AK-47 FDTD mesh with 2-mm resolution (the tick marks on the axes represent numbers of FDTD cells).

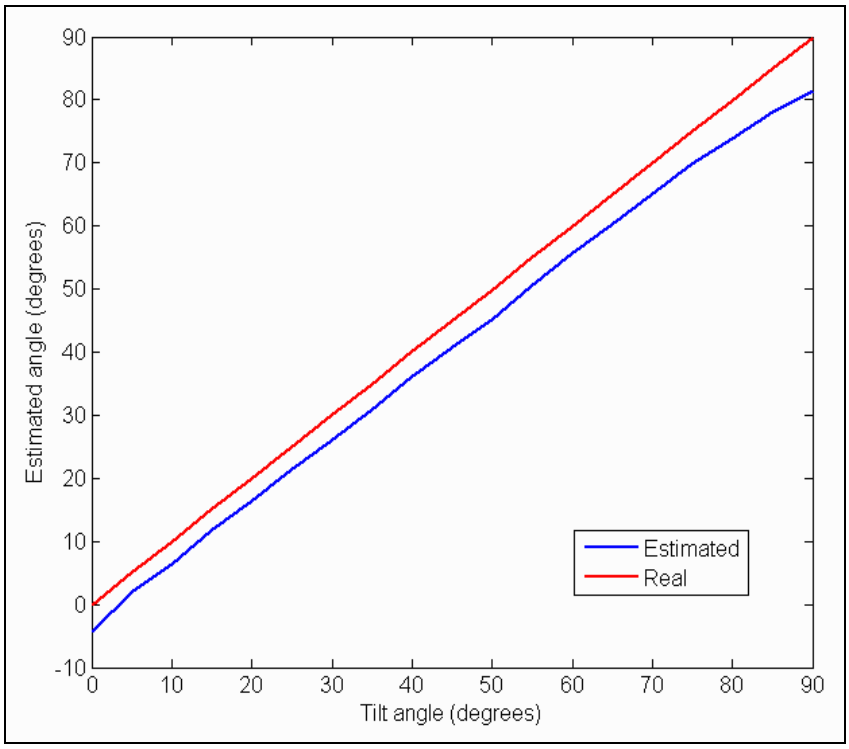

Figure 4. Estimating the tilt angle of the AK-47 rifle using the procedure described in section 2.

As a further step, we look at the enhancement in the radar cross section (RCS) when we use the S_{11}^{opt} element instead of the vertical-vertical (V-V) or horizontal-horizontal (H-H) elements of the scattering matrix (figure 5). Obviously, the RCS improvement is dependent of the rifle tilt angle: at 0° tilt (vertical position), the V-V polarization yields the maximum response; whereas, at 90° tilt (horizontal position), the H-H polarization yields the maximum response. As expected, using the S_{11}^{opt} element produces the same RCS no matter the tilt angle. The largest RCS improvement is noticed at 45° tilt and is about 4 dB. Again, the results were averaged over the 0.5 to 2.5 GHz band.

Although this polarization-dependent optimization of the radar signature seems to work well for a rifle-like object in free space, adding other targets with large signature in the vicinity of the object of interest can dramatically change the polarization dependence of its radar response. In particular, if the rifle is carried by a human (whose radar signature is largely polarization independent), the procedure described previously does not enhance the radar signature. The reason for this is that the rifle return is mostly obscured by the much larger human body signature. To illustrate this, we tried to estimate the rifle tilt angle in the presence of a human body, similarly to the procedure described in figure 4. The new results are shown in figure 6 and they indicate that our signature optimization attempt failed in this case. In general, we expect this procedure to be very sensitive to clutter (such as that produced by a human body), which renders it mostly useless in a real-life weapon detection scenario. Moreover, if the scenario involves two

or more rifles oriented at different tilt angles with respect to the radar line of sight, the polarization-dependent optimization procedure cannot work either. Section 3 will describe a more robust approach for the weapon detection problem, also based on polarimetric techniques.

Note: Throughout this report, we use the human body model of the "fit man," which was described in reference 1. This is a realistic computer mesh, where we modeled the body as a uniform dielectric with $\varepsilon_r = 50$ and $\sigma = 1$ S/m (see reference 1 for more details on the validity of this model).

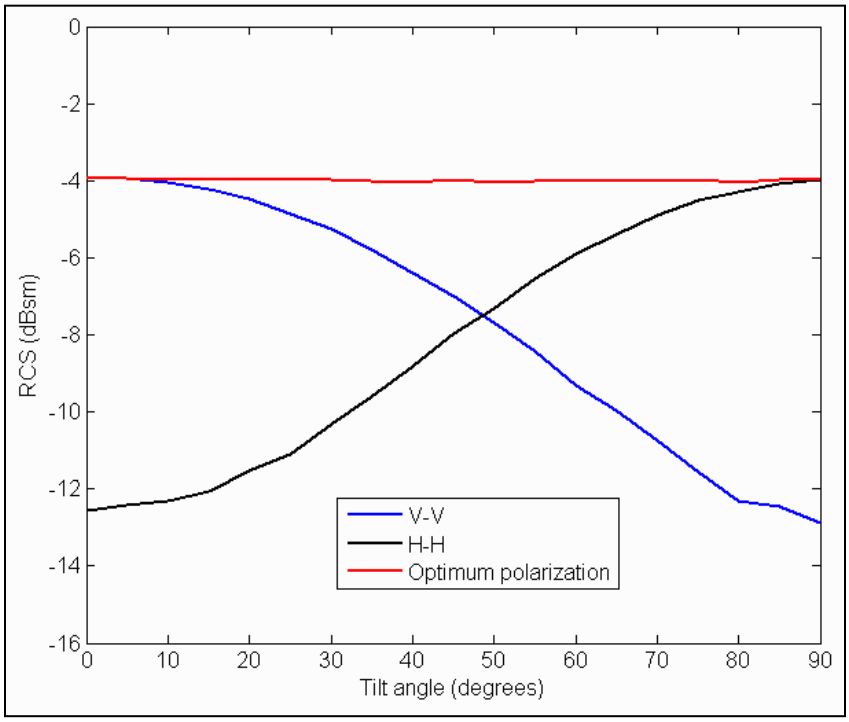

Figure 5. RCS of the AK-47 versus tilt angle showing the improvement obtained by the polarization optimization procedure described in section 2.

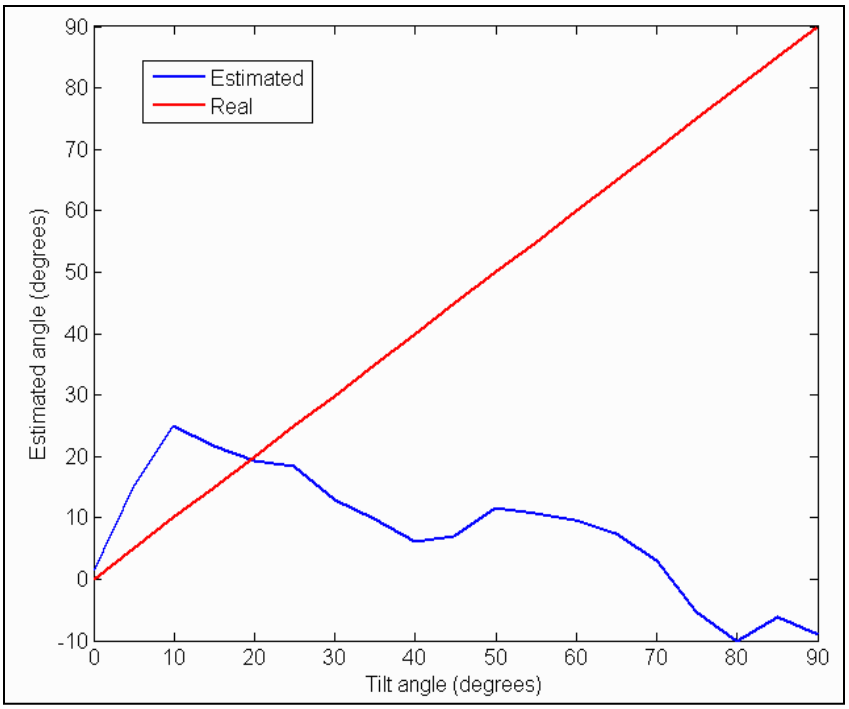

Figure 6. Attempting to estimate the tilt angle of the rifle carried by a human by the procedure described in section 2.

3. Using the Cross-Polarization Signature for Target Discrimination

3.1 Basic Approach

The approach introduced in this section is based on the observation that a rod-like object oriented at a tilt angle from the vertical and horizontal axes has a relatively strong cross-polarization response. Consider an idealized such object placed in vertical position. To simplify the formulation, we assume that the scattering matrix in this case has only one non-zero element, S_{vv}. Now consider that we rotate the object by an angle α, which is equivalent to rotating the coordinate system (in the **E** vector plane) by an angle $-\alpha$. With the rotation matrix **R** given by equation 7, the scattering matrix can be written in the new (rotated) coordinate system as

$$\mathbf{S}^{tilt} = \mathbf{R}^{*}\mathbf{S}\mathbf{R}^{T} = \begin{bmatrix} \cos\alpha & -\sin\alpha \\ \sin\alpha & \cos\alpha \end{bmatrix} \begin{bmatrix} S_{vv} & 0 \\ 0 & 0 \end{bmatrix} \begin{bmatrix} \cos\alpha & \sin\alpha \\ -\sin\alpha & \cos\alpha \end{bmatrix} = \begin{bmatrix} \cos^2\alpha\, S_{vv} & \cos\alpha\sin\alpha\, S_{vv} \\ \cos\alpha\sin\alpha\, S_{vv} & \sin^2\alpha\, S_{vv} \end{bmatrix} \quad (9)$$

Thus, the target exhibits a sizeable cross-polarization response relative to the new coordinates in the **E** vector plane. It is easy to see that the cross-polarization elements reach a maximum when $\alpha = 45°$. Also, in the new coordinate system, the ratio of the cross- to co-polarization elements

(for instance, S_{vh}^{tilt} and S_{vv}^{tilt}) is $\tan\alpha$. This is in contrast with targets that do not exhibit a preferential axis, these targets generally have a low cross- to co-polarization ratio that is not sensitive to a rotation in the **E** vector plane.

We illustrate this idea by computing the RCS of a standing human carrying an AK-47 rifle in the port-arm position (figure 7a). In this case, the rifle is tilted at 45°, and the radar elevation angle is 0° (propagation in the *x*-*y* plane). The values displayed in figures 7b through 7d represent RCS averaged over a 400-MHz frequency band centered at 1 GHz (the averaging procedure basically eliminates some deep nulls in the RCS curves that would appear at specific frequencies and aspect angles). The RCS of the human with and without rifle for V-V polarization is shown in figure 7b, while figure 7c looks at the RCS for vertical-horizontal (V-H) polarization. From these graphs we infer that the cross-polarization response of the tilted rifle is much stronger than that of the human body. At the same time, the co-polarization return from the human body is not significantly altered by the presence of the rifle. In order to discriminate between the two scenarios, one would take the ratio (difference in dB) between the cross- and co-polarization signatures and compare that to a threshold (established through some calibration procedure). Although it is obvious that at 0° azimuth (when the human faces the radar) the cross- to co-polarization ratio is much larger for the human carrying the rifle (since the human himself is mostly symmetric at this aspect angle, making its cross-polarization signature very low), the difference between the ratios in the two scenarios is still significant for most other aspect angles (figure 7d). Notice that, for azimuth angles beyond −90° or 90°, there is not much difference between the two scenarios, because for those angles the rifle is masked by the body. Interestingly, as shown in section 3.2, we found out that the strong cross-polarization signature of the rifle holds for virtually any tilt angle.

3.2 Images of a Human Carrying a Rifle in Free Space

In this section, we take the analysis one step further by creating synthetic aperture radar (SAR) images of the human with and without a rifle in free space. The SAR images are based on integrating FDTD simulated radar range profiles over a large range of frequencies (2-GHz bandwidth centered at 2.5 GHz) and azimuth angles (30° aperture centered at broadside). The scattering models are performed in the far-field (at 0° elevation) and the polar format algorithm (*13*) is employed in image formation. The images represent two-dimensional pseudo-color maps with downrange on the *x*-axis and cross-range on the *y*-axis. In all images, the human faces left, while the radar looks from the left side. The intensity scales are always in dB. More details on this procedure can be found in reference 2.

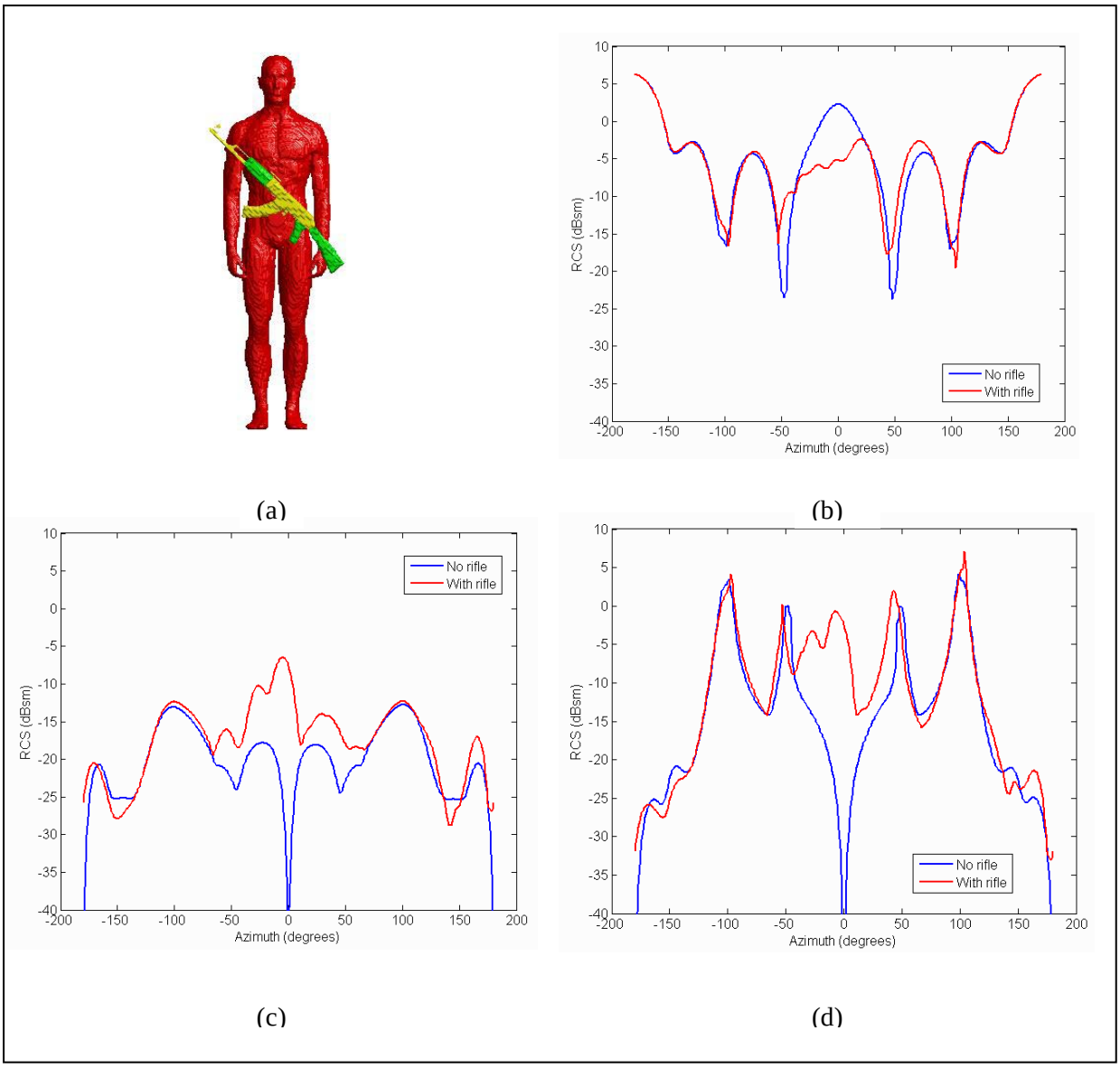

Figure 7. RCS of the standing human with and without a rifle versus azimuth angle showing: (a) the computational mesh, (b) RCS for V-V polarization, (c) RCS for V-H polarization, and (d) V-H to V-V RCS ratio.

We consider four cases: the man without a rifle, and the man carrying a rifle at 0°, 45°, and 90° tilt angles. Figure 8 shows the SAR images obtained for these cases for V-V polarization (H-H polarization for the 90° tilt), whereas figure 9 shows the images obtained for V-H polarization. The intensity of the brightest pixel in every image is marked in the figures. Based on these results, we notice that the cross- to co-polarization ratio of the brightest pixel is –23 dB for the human without rifle and between –13 to –15 dB for the human with rifle. Therefore, there is a gain of at least 8 dB in this ratio when the rifle is present, which can be exploited in a weapon detection scheme. The reason why the rifle still exhibits a relatively strong cross-polarization response at 0° and 90° tilt is not entirely clear to us at the time of this investigation. It is possible that, in these cases, the bullet magazine is mainly responsible for the cross-polarization signature.

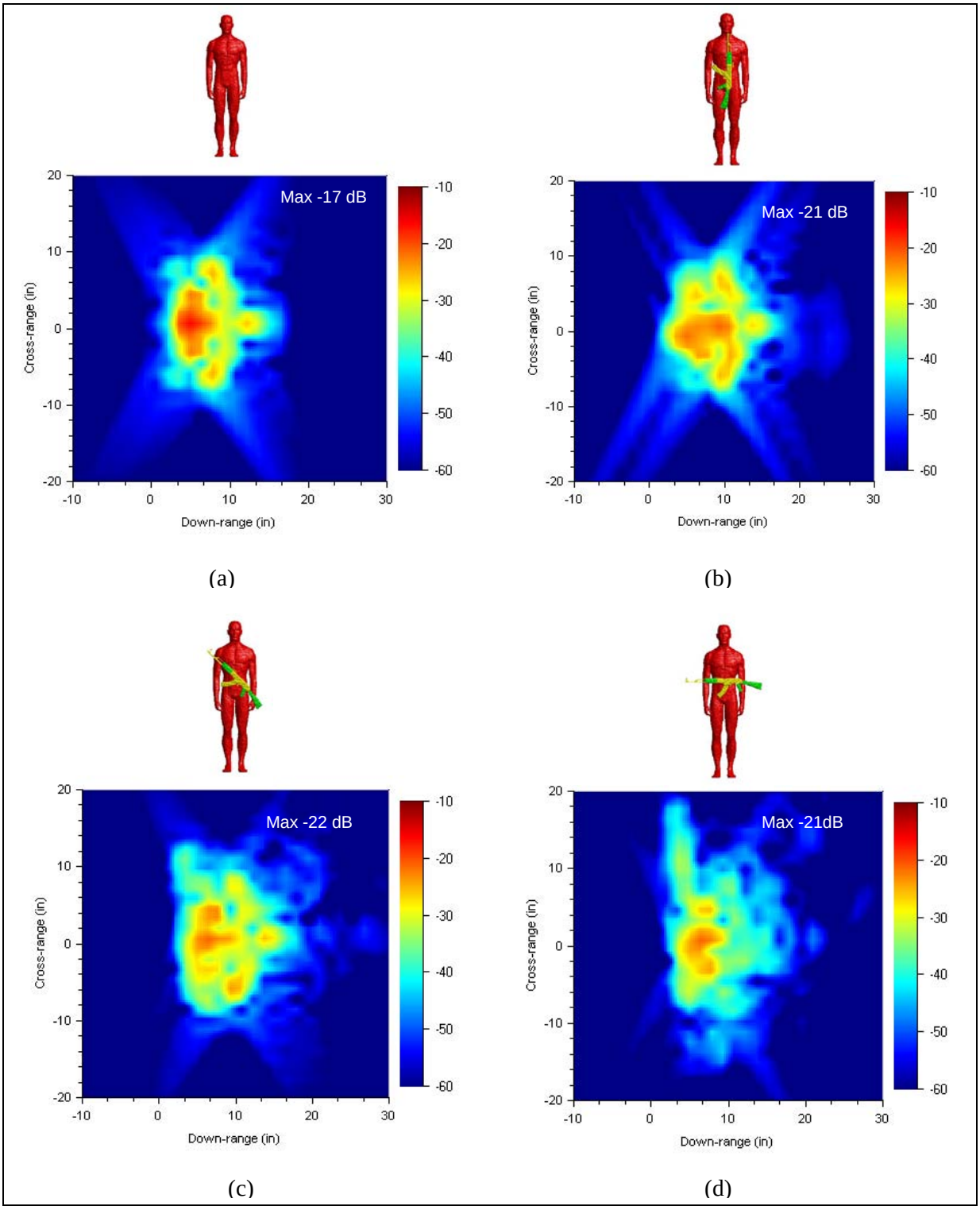

Figure 8. Co-polarization SAR images of a human with and without a rifle showing: (a) human without rifle, V-V polarization; (b) human with vertical rifle, V-V polarization; (c) human with rifle tilted at 45°, V-V polarization; and (d) human with horizontal rifle, H-H polarization.

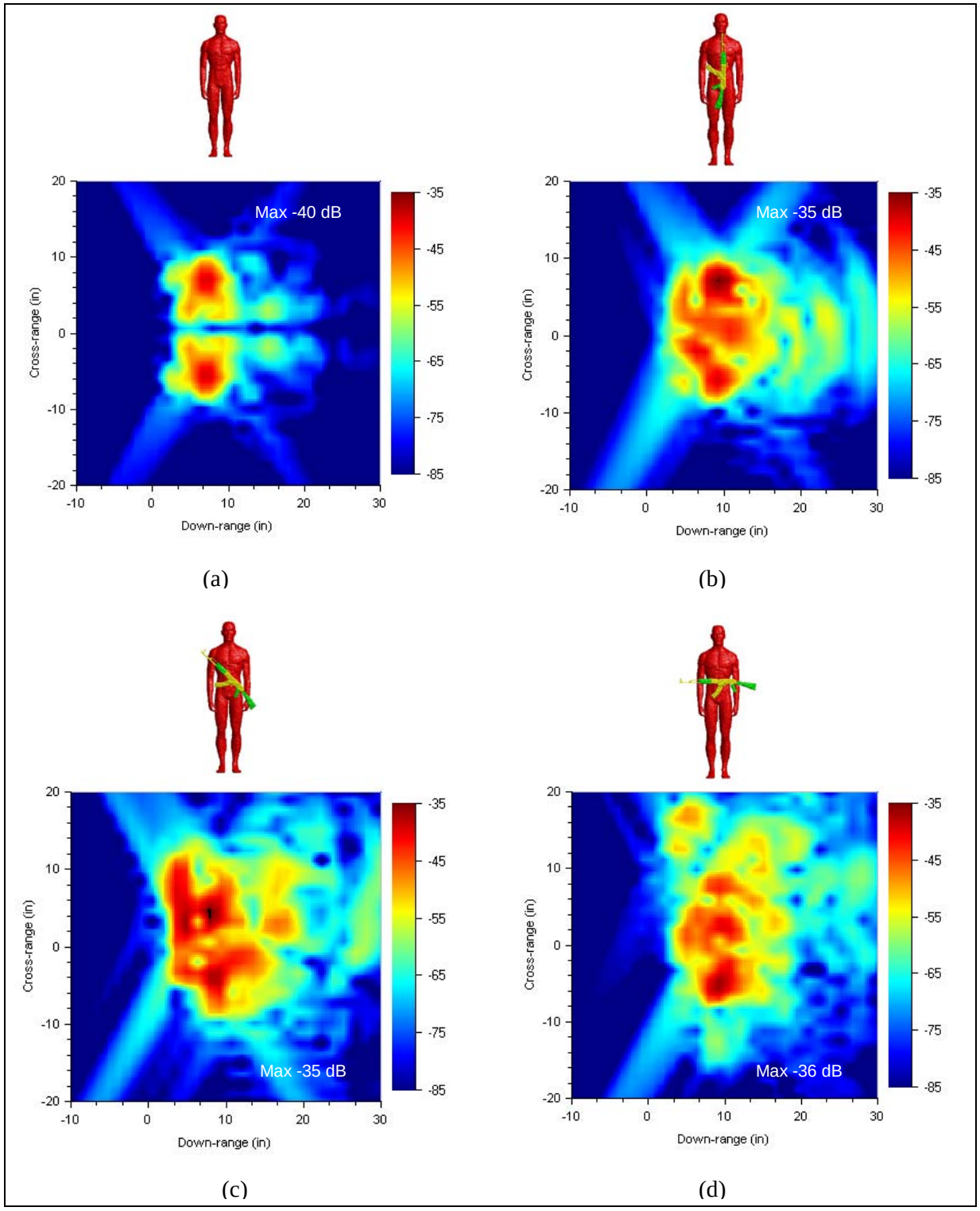

Figure 9. Cross-polarization (V-H) SAR images of a human with and without a rifle showing: (a) human without rifle, (b) human with vertical rifle, (c) human with rifle tilted at 45°, and (d) human with horizontal rifle.

3.3 Images of a Human Carrying a Rifle Behind Walls

The purpose of this study is to investigate weapon detection techniques for concealed environments, in particular, for through-the-wall radar sensors. In this section, we place the human and rifle targets in a room or a building and apply the ideas presented previously to detect the presence of weapons. It is interesting to mention that, as shown in reference 2, the walls are mostly absent from the cross-polarization image. This makes the cross-polarization mode well suited in rejecting the walls, while emphasizing the human targets and possible weapons.

The room imaging techniques used in this section are the same as those described in reference 2. The scattering data is based on computer modeling of the radar return. We use far-field geometry, with an elevation angle of 0°. The entire room is placed in free space, meaning there is no infinite ground plane underneath the walls. However, we add a flat ceiling and a floor with the exact same extent as the room perimeter. The polar format algorithm (*13*) is used in the image formation process. As in section 3.2, the images represent two-dimensional pseudo-color maps with downrange on the *x*-axis and cross-range on the *y*-axis (the radar looks from the left side). The mesh contours are overlaid onto the SAR images in gray to help locate the objects in the scene.

The radar return computations were performed with the AFDTD code. All the meshes in this section have a resolution of 5 mm (discussions on the model accuracy can be found in reference 4). We consider two room sizes: one has dimensions 5 m by 3.5 m by 2.2 m (197 in by 138 in by 87 in), while the other has dimensions 10 m by 7 m by 2.2 m (197 in by 138 in by 87 in). These represent very large meshes that can only be handled by large computer clusters running a parallel version of the AFDTD code. Thus, the larger of the rooms includes 1.68 billion cells and the simulation at one incidence angle requires 128 processors. Overall, obtaining one image of the large room took about 500,000 central processing unit (CPU) hours. All the simulations were performed at the U.S. Army Major Shared Resource Center (MSRC) (*14*) on Linux Networx Evolocity II clusters. The images were created with the Pioneer RCS software on desktop personal computers running Windows XP.

First, we consider the simple (smaller) room that is represented in figure 10. The walls are 8 in thick, made of brick, with $\varepsilon_r = 3.8$ and $\sigma = 0.03$ S/m (*2*). The ceiling and floor are represented as 6-in-thick concrete slabs, with $\varepsilon_r = 6.8$, $\sigma = 0.1$ S/m. The fit man is placed in the middle of the room. The AK-47 rifle is carried at a tilt angle of 45°. The SAR images involve an effective bandwidth of 2 GHz centered at 2.5 GHz and an effective aperture of 30° centered at broadside (we use Hanning windows in both the frequency and angular domain). The images obtained for this room for V-V polarization are shown in figure 11: (a) human without rifle and (b) human with rifle. The differences between the two images are very small (the brightest pixels in various image areas are marked in the figure). However, if we look at the images obtained for V-H polarization (figure 12), we notice that the human carrying a rifle (b) is much brighter than that without a rifle (a). (Note: The second image that appears behind the correct position of the

human is an artifact called “ghost image” and was explained in reference 2.) The cross- to co-polarization ratio for the brightest pixel in the human image is −24 dB for the case without rifle and −16 dB for the case with rifle. Again, we find a difference of 8 dB between the two cases.

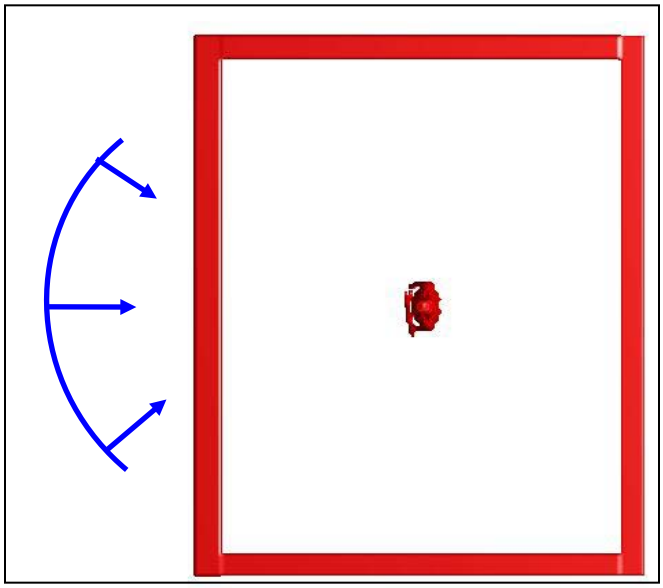

Figure 10. Top view of the simple brick wall room showing a human carrying an AK-47, with the radar moving along a circular arc in the far-field, on the left side in the figure.

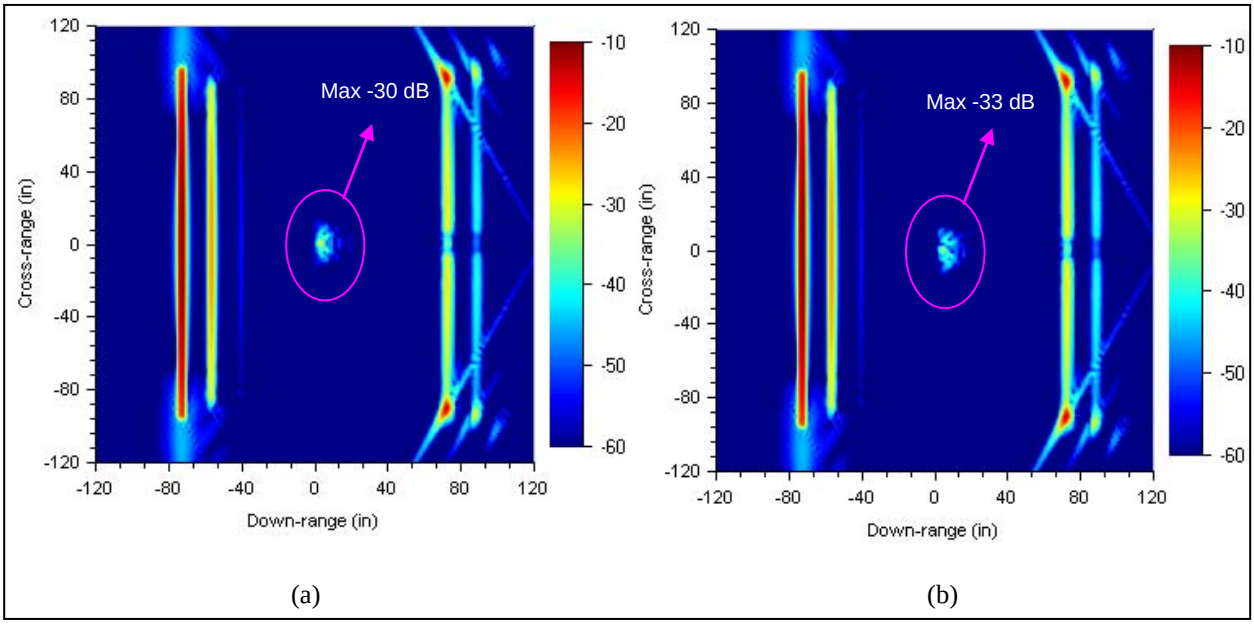

Figure 11. Co-polarization (V-V) SAR images of a human placed in the middle of a brick wall room showing (a) human unarmed and (b) human with AK-47.

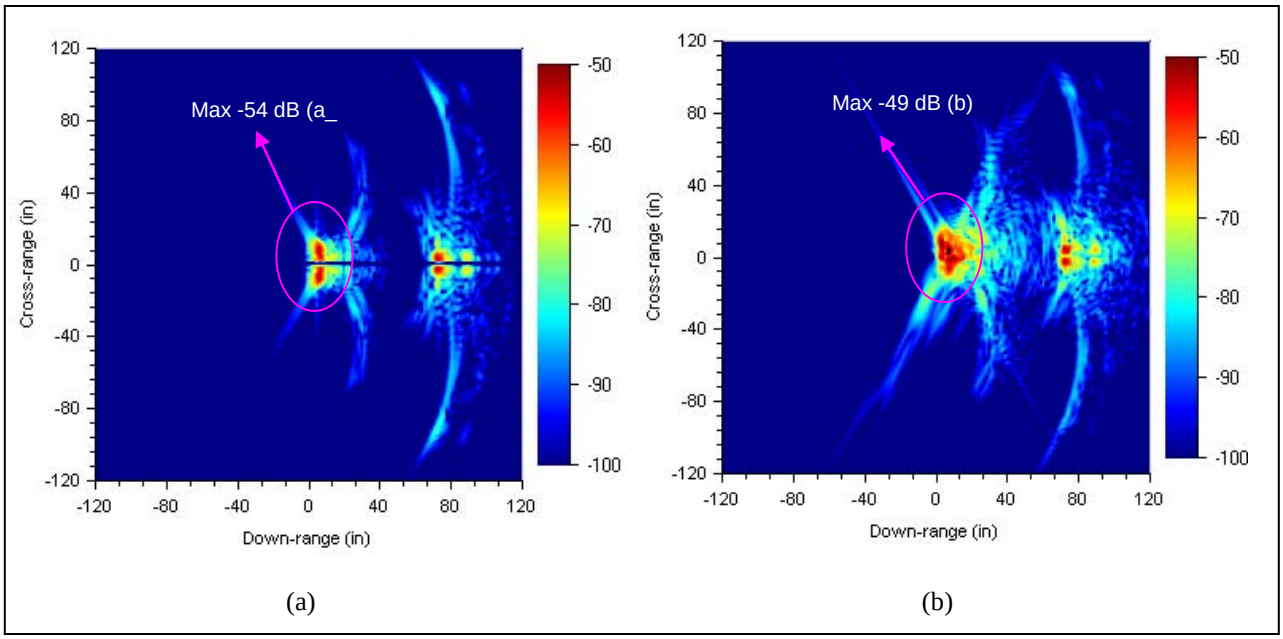

Figure 12. Cross-polarization (V-H) SAR images of a human placed in the middle of a brick wall room showing (a) human unarmed and (b) human with AK-47.

Next, we create the SAR images of the complex room represented in figure 13. The exterior walls are made of 8-in brick and are equipped with glass windows and a wooden door. There is also an interior wall made of 2-in-thick sheetrock (equipped with a door as shown in the figure). There are four humans in this mesh, placed at different azimuth orientation angles and tagged with labels 1 through 4, as in figure 13b. We added the following furniture objects: a bed, a couch, a bookshelf, a dresser, and a table with four chairs. These objects are made primarily from wood (except for the mattress and cushions where we used some generic fabric material). We also included 2-in-thick concrete slabs as ceiling and floor. The rifles (when present) are tilted at 45°. All the objects included in this mesh were obtained by conversion from realistic computer aided design (CAD) models of the respective objects. Details on the dielectric properties of the materials used in the mesh can be found in reference 2. The SAR images are created using an effective bandwidth of 1.1 GHz centered at 1.4 GHz and an aperture of 30° centered at broadside on two sides of the building.

As mentioned in section 3.1, the strong contribution of the rifle to the cross-polarization signature of the human is evident only when the radar can “view” the rifle directly (the rifle is not masked by the human body). In order to achieve good aspect angle diversity, we image the room from two sides (left and bottom), meaning that we integrate separate apertures centered at broadside on two sides of the building. For the purpose of illustrating the discrimination technique, we placed the rifles on humans in positions that are favorable to the imaging scenario, such that the radar has direct line of sight to each rifle from either side of the building. If the

radar could not see the rifle directly, then the discrimination procedure would not work. The angles between the humans' boresight directions and the *x*-axis are as following: (1) 45°, (2) 0°, (3) 10°, and (4) –20°.

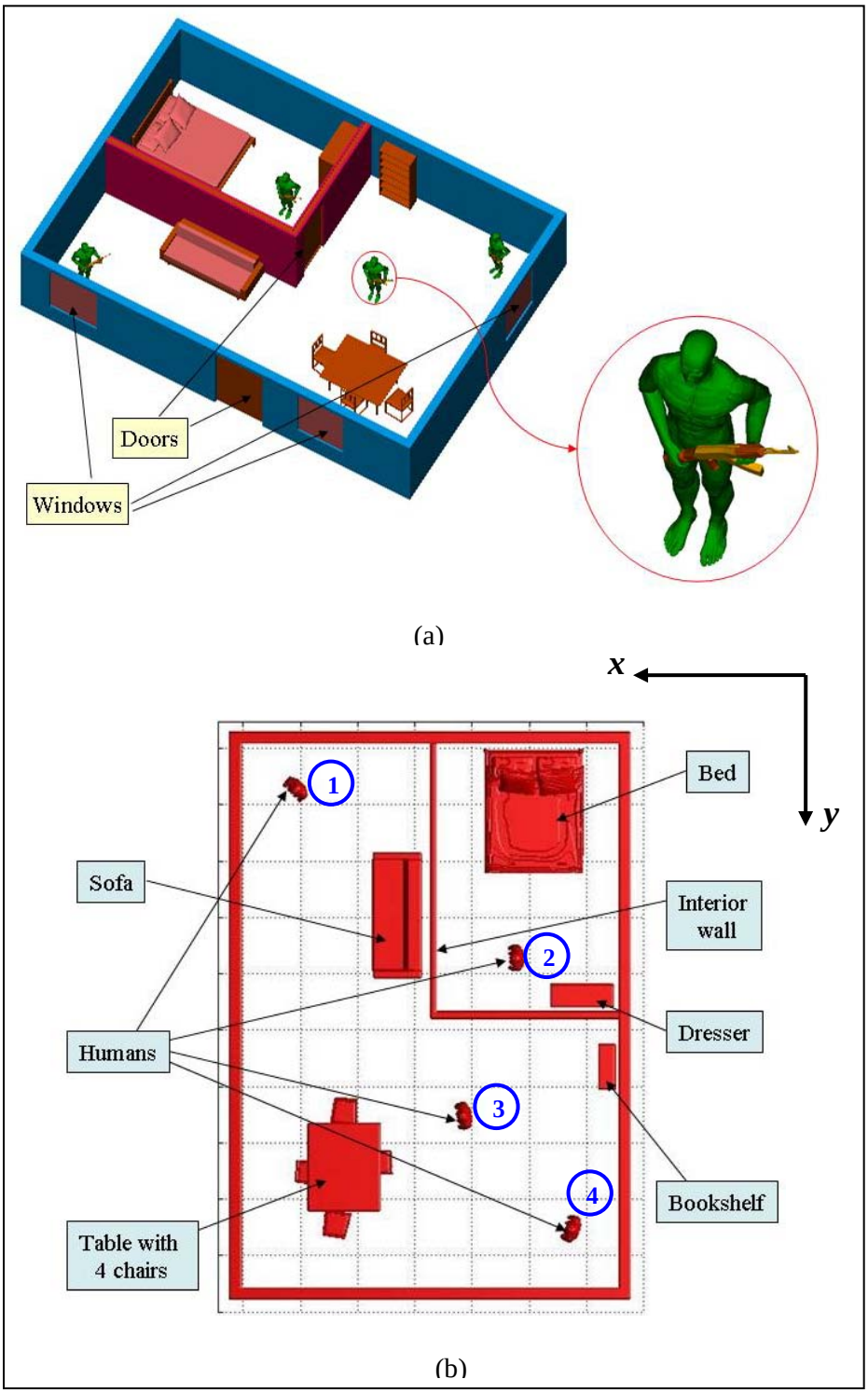

Figure 13. The complex room containing humans and furniture objects showing (a) perspective view (humans carrying rifles) and (b) top view (humans unarmed).

The images of the complex room are shown in figures 14 and 15. We present the images taken from the left and bottom sides separately. A top view of the mesh is overlaid on top of the images (in gray contours) in order to help with image interpretation. The images in figure 14 show the V-V polarization as follows: (a) no rifles, radar on left side of the building; (b) with rifles, radar on left side of the building; (c) no rifles, radar on bottom side of the building; and (d) with rifles, radar on bottom side of the building. In figure 15, we show the same images obtained for V-H polarization. The maximum pixel intensities in the human areas are marked in the figures. Qualitatively, one can notice an increase in brightness in the cross-polarization images when the rifles are present, with increases in the cross- to co-polarization intensity ratios consistent with the previous results. The enhancement in the cross-polarization images is more evident when the aperture is placed on the left side of the page, since, in that case, the radar can "see" the rifles at angles close to broadside (figure 15a and b). When the aperture is placed at the bottom side of the page, the human bodies partially block the rifles and consequently the cross-polarization enhancement effect is significantly reduced (figure 15c and d). Other interesting effects in the images shown in figures 14 and 15 (such as the presence of ghost images of humans projected on walls behind them) were explained in reference 2 and are not particularly relevant to our problem.

We summarize all the quantitative results from the images presented in sections 3.2 and 3.3 in table 1. In this table, we record the brightest pixel in the image area around each human for the cases with and without rifle, for co- and cross-polarization. Then we calculate and compare the cross- to co-polarization ratios for all these cases. We notice that in most cases this ratio is consistently at least 8 dB larger for the case when the human carries a rifle. Therefore, this metric can be used in a discrimination procedure that searches for humans carrying this type of weapon.

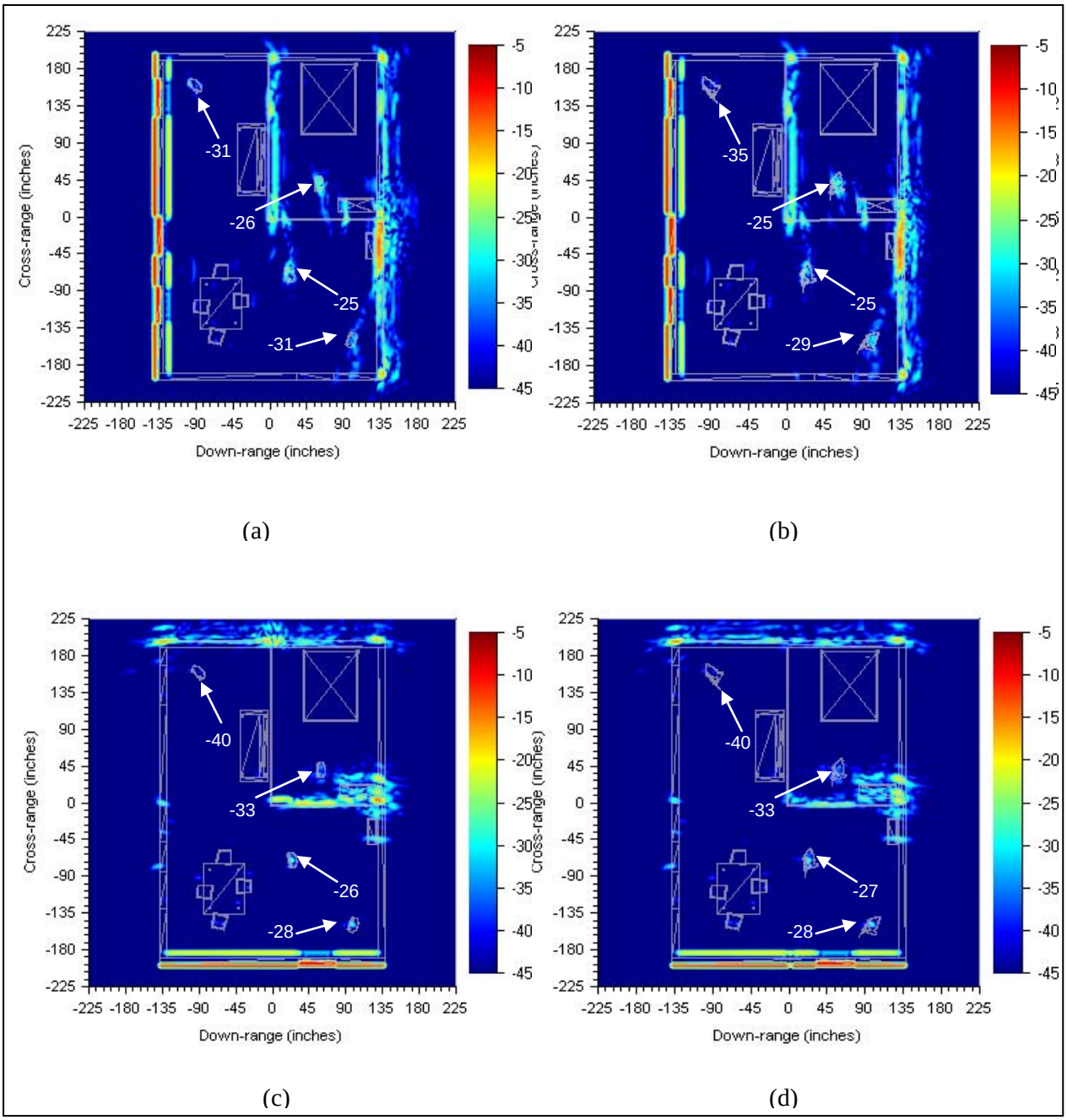

Figure 14. Co-polarization (V-V) SAR images of the complex room in figure 13 showing: (a) aperture on left side, humans without rifles; (b) aperture on left side, humans with rifles; (c) aperture on bottom side, humans without rifles; and (d) aperture on bottom side, humans with rifles.

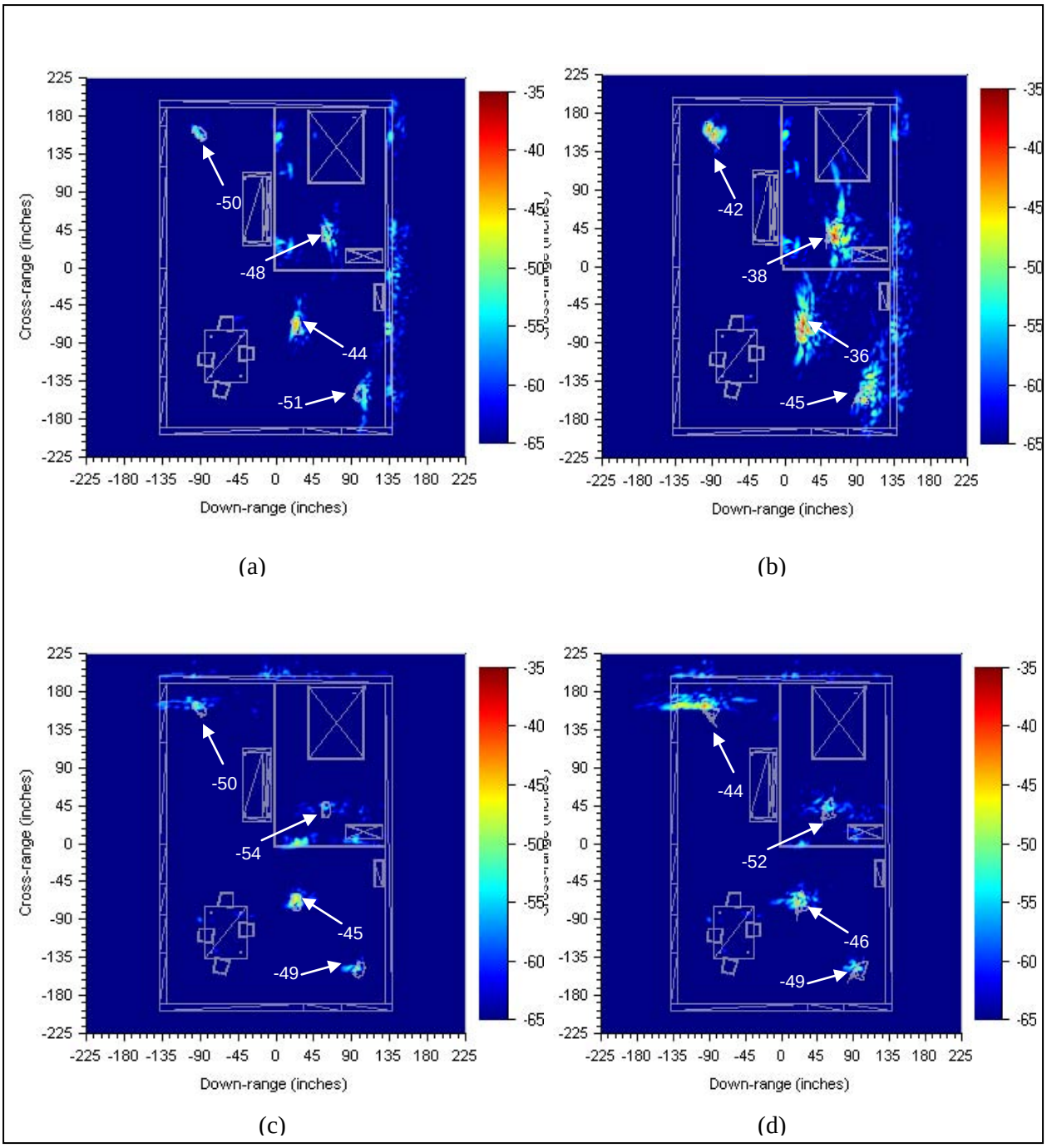

Figure 15. Cross-polarization (V-H) SAR images of the complex room in figure 13 showing: (a) aperture on left side, humans without rifles; (b) aperture on left side, humans with rifles; (c) aperture on bottom side, humans without rifles; and (d) aperture on bottom side, humans with rifles.

Table 1. Comparison of maximum pixel intensity in the human areas within the SAR images presented in sections 3.2 and 3.3, in co- and cross-polarization, for the cases with and without rifle (all values in dB).

		Max Pixel	No Rifle	Rifle Tilt Angle		
				0°	45°	90°
Free-space		Co-pol	–17	–21	–22	–21
		Cross-pol	–40	–35	–35	–36
		Ratio	–23	–14	–13	–15
Simple room		Co-pol	–30		–33	
		Cross-pol	–54		–49	
		Ratio	–24		–16	
Complex room	Human #1	Co-pol	–31		–35	
		Cross-pol	–50		–42	
		Ratio	–19		–7	
	Human #2	Co-pol	–26		–25	
		Cross-pol	–48		–38	
		Ratio	–22		–13	
	Human #3	Co-pol	–25		–25	
		Cross-pol	–44		–36	
		Ratio	–19		–11	
	Human #4	Co-pol	–31		–29	
		Cross-pol	–51		–45	
		Ratio	–20		–16	

3.4 Rifle Detection Algorithm Based on SAR Images of Rooms

In this section, we develop a behind-the-wall weapon detection algorithm based on the simulated SAR images in section 3.3. The decision is made by comparing the pixel-by-pixel map of the metric developed in the previous sections (the cross- to co-polarization signature ratio) with a threshold. The threshold is established by studying the metric's probability distribution function obtained for simulated SAR images.

Consider the images in figures 14a and b and 15a and b (the complex room imaged from the left side). Before we compute the pixel-by-pixel cross- to co-polarization ratio map, we need to make sure that very low intensity pixels in the original images (which represent noise and can take random values) are not directly used in building the ratio map. Thus, we assign to every pixel in the original images below a certain threshold (–40 dB in the co-polarization images and –60 dB in the cross-polarization images) the value of that threshold. The thresholds were chosen by direct examination of the SAR images in figures 14a and b and 15a and b, such that all the targets of interest appear with intensities above those numbers. We also need to make sure that the "noise" pixels display a cross- to co-polarization ration below the detection threshold.

After the pre-screening procedure we build the pixel-by-pixel cross- to co-polarization ratio map. The probability distribution functions (PDF) of the ratio for the cases without rifles (figures 14a and 15a) and with rifles (figures 14b and 15b) are shown in figure 16. Notice that the PDF is always based on pixel intensities on linear (not dB) scales. The plots in figure 16 clearly demonstrate that there are more pixels with a high cross- to co-polarization ratio for the case with rifles, whereas for the case without rifles this ratio never exceeds 0.6. If we choose a detection threshold of −10 dB (corresponding to about 0.3 on linear scale), we obtain the detection maps in figure 17. Here, we notice that all four humans carrying rifles are detected correctly (figure 17b), but we also obtain a false alarm in the image representing humans without rifles (figure 17a). If we increased the detection threshold (say to 0.6 on linear scale), we would eliminate the false alarm, but in that case we would also miss detecting the rifle on human #4 in figure 17b.

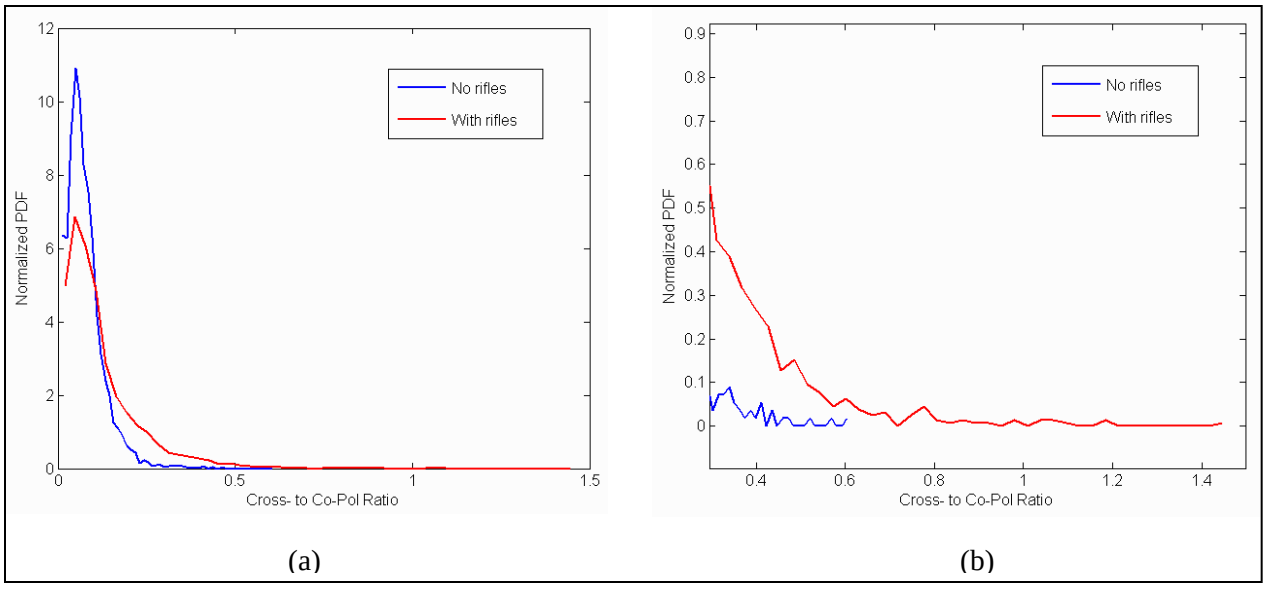

Figure 16. Normalized probability distribution functions of the pixel-by-pixel cross- to co-polarization ratio in the complex room SAR images obtained from the left side, showing (a) the entire distribution and (b) detail of the distributions' tails.

Notes: • Only pixels above −40 dB for co-polarization and above –60 dB for cross-polarization were considered in these distributions.
• The pixel intensities were converted to linear scale.

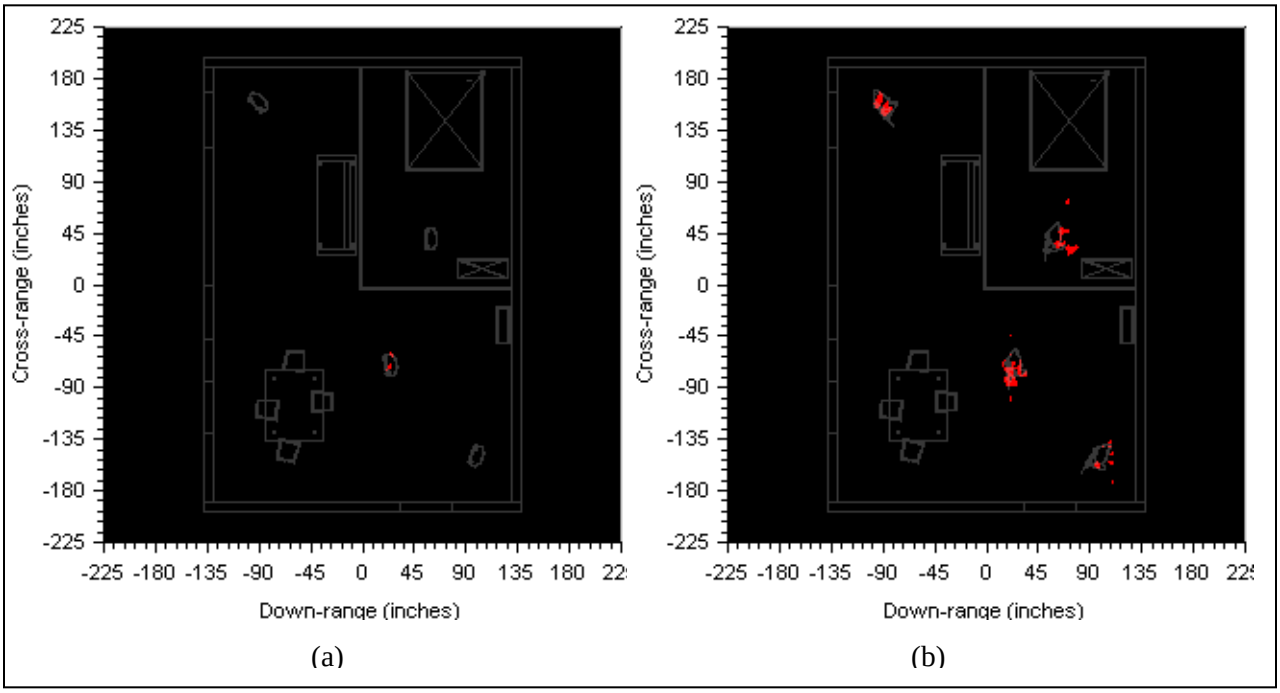

Figure 17. Detection maps for the complex room in figure 13 based on thresholding the cross- to co-polarization ratio, for the cases where (a) the humans carry no rifles and (b) the humans carry AK-47 rifles.

Note: In this case, the thresholding procedure was applied directly to the pixel maps in figures 14a and b and 15a and b.

There are certain refinements that can be applied to the detection procedure outlined previously. For instance, a constant false alarm rate (CFAR) (*15*) algorithm can be employed in adaptively setting the detection threshold within the SAR image. Another technique, which we demonstrate here, "smears" the original SAR images by means of a moving average spatial filter, in order to eliminate spurious spikes that can lead to false alarms (*16*). It turns out that the images shown in figures 14 and 15 have very fine pixel size (1.9 by 1.9 cm), which is much below the expected image resolution (about 15 by 20 cm). In order to eliminate spurious pixel variations within a resolution cell, we apply a square moving average filter with size 10-by-10 pixels to the original cross- and co-polarization SAR images. We then create the new detections maps via the algorithm presented earlier in this section, this time setting the detection threshold at –15 dB (since the entire cross- to co-polarization ratio PDF is modified by the pixel averaging procedure). As seen in figure 18, all four humans carrying rifles are now clearly detected in the SAR image, whereas all false alarms (for the case of personnel without rifles) are eliminated (since for that case the detection map is blank, it is not shown here).

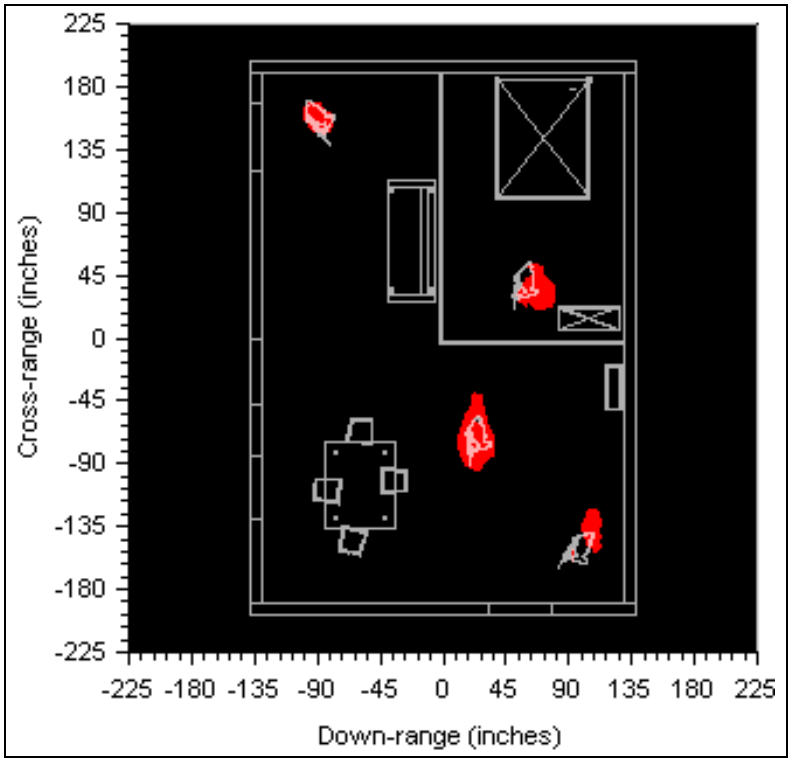

Figure 18. Detection map for the complex room in figure 13 containing humans with rifles, obtained after applying a pixel averaging procedure to the images in figures 14a and b and 15a and b.

In practice, a radar system would need extensive training data in order to determine the detection algorithm parameters, such as the pre-screening and detection thresholds or the pixel averaging filter size. These would depend on the specific radar system and imaging parameters, but should be relatively constant for various target classes. Subject to further investigation, we conjecture that most common objects encountered in a STTW scenario exhibit a low cross- to co-polarization signature ratio that is significantly below the ratio displayed by a rifle-like object. We also expect this result to hold independently from wall attenuation, clutter, or noise level in the image. Another important assumption which needs to be verified is that the cross- to co-polarization ratio is relatively stable (within a few dB) for the radar signature of humans of various sizes and shapes.

3.5 Doppler Spectrum of a Walking Human Carrying a Rifle

In reference 5, we investigated the Doppler spectrum of walking human carrying an AK-47. We compared the Doppler spectrograms obtained in that case with those of a human walking without any weapon. We noticed some slight difference between the two cases, mainly the fact that the arm swinging (high velocity components in the spectrogram) does not show up in the case where the human carries the rifle. However, while the arm swinging motion can be clearly detected in a Doppler spectrogram, its absence does not necessarily indicate the presence of a weapon (the

human may walk with the hands in the pockets, for instance). A more reliable method for rifle detection by Doppler radar would exploit the same polarimetric signature differences as explained in section 3.1.

In this section, we perform the analysis of the Doppler signature outlined in reference 5, by modeling the frame-by-frame radar return from a human in walking motion. After computing the in-phase-quadrature (I-Q) samples corresponding to each received pulse, we take a Fourier transform across the slow time in order to obtain the Doppler spectrum. The human walks straight at the radar (the azimuth and elevation angles are both 0°). In this example, the human is placed in free space. The motion of the human carrying the AK-47 differs from that of the free walking motion (figure 19a) only by the fact that the arms are fixed, as shown in figure 19b (the rest of the body, including the head, torso, and legs, has the same frame-by-frame position). In this section, we simply compute the cross- to co-polarization ratio of the Fourier transform magnitudes (there is no need to perform a time-frequency analysis such as in reference 5). The length of the Fourier transform is not critical in this case—we consider the I-Q data characterizing one full walking cycle. Other parameters relevant to the problem are as follow: walking cycle period, 2 s; average velocity of the human, 0.6 m/s; center frequency, 1 GHz; bandwidth, 80 MHz; coherent processing interval, coherent processing interval (CPI) = 0.3 s; and pulse repetition frequency, PRF = 40 Hz.

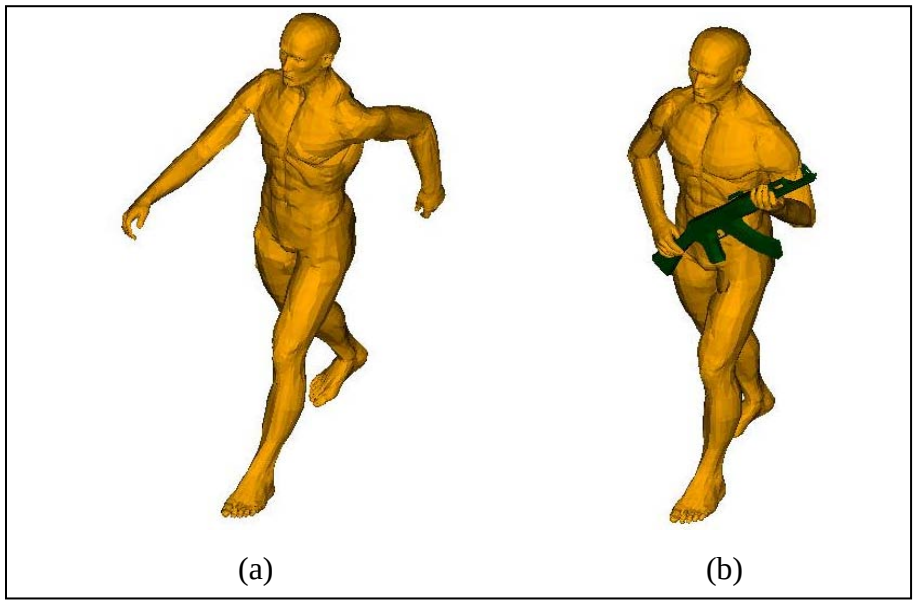

Figure 19. Human body mesh in walking motion showing (a) free walking motion and (b) walking with an AK-47.

The plots in figure 20 show the Doppler spectrum for V-V polarization (a), the V-H polarization (b), and the difference (in dB) between the V-H and V-V magnitudes (c) for both the walking human carrying a rifle and not carrying a rifle. Notice that, before we plot the difference between V-H and V-V magnitudes, we threshold out the spectrum data below −40 dB (for V-V) and −55 dB (for V-H), in order to eliminate spurious data points that characterize the difference between very low signal levels. The graphs in figure 20c show that, for the main part of the Doppler spectrum (between 0 and 1 m/s), the V-H to V-V ratio is significantly larger for the human carrying a rifle than for the human without a rifle. However, the Doppler response at the edges of the spectrum (between −0.5 to 0 m/s and between 1 and 2 m/s) shows a larger V-H to V-V ratio for the human without a rifle, which can be explained by the dominance of the swinging arm response in those regions of the spectrum.

We should mention here that the large cross- to co-polarization ratio difference between the two cases at 0° azimuth angle is easily explained by the simple fact that the human body alone is a highly symmetric target at this aspect angle; therefore, its cross-polarization signature is very low (in fact, the only asymmetry is introduced by the arm and leg motion; however, the dominant response comes from the torso which is exactly symmetric in the model). Therefore, we need to examine a more challenging case, such as when the azimuth angle is 30° (figure 20d). Even for that case, we notice a similar pattern in the cross- to co-polarization ratio, namely, a significantly larger ratio for the case with weapon in the main part of the Doppler spectrum.

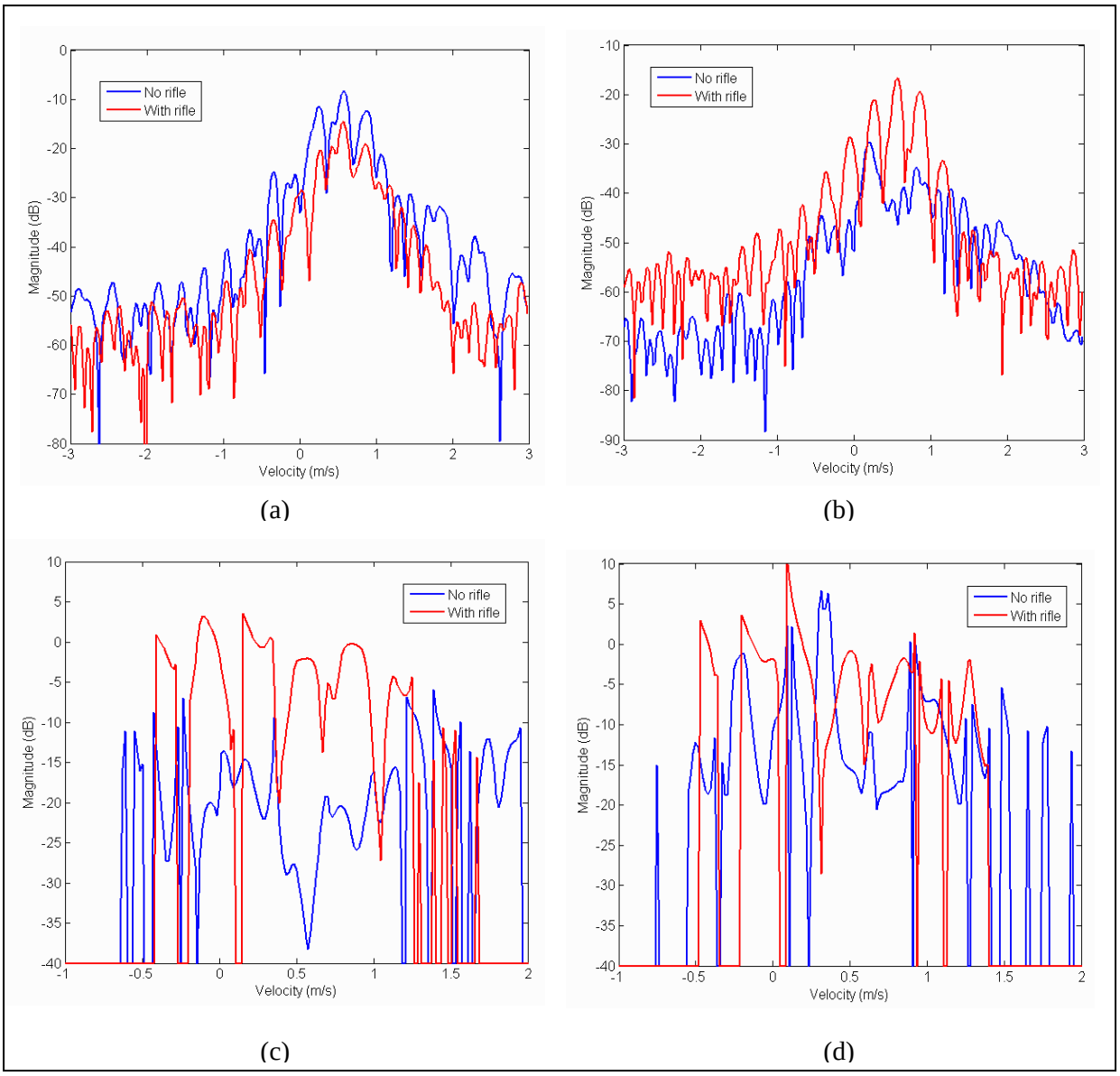

Figure 20. Doppler spectrum of a human walking with and without a rifle showing: (a) V-V polarization, 0° azimuth; (b) V-H polarization, 0° azimuth; (c) V-H to V-V ratio, 0° azimuth; and (d) V-H to V-V ratio, 30° azimuth.

3.6 Human Carrying a Rocket Propelled Grenade

In this section, we examine another target of interest, the RPG. Here, we call an RPG the entire assembly formed by the rocket-propelled grenade together with the launcher. Similarly to a rifle, this object exhibits a large shape factor; therefore, the same polarimetric radar techniques should apply in this case. Since we already proved that the cross- to co-polarization ratios of the target images are largely preserved upon transmission through a homogeneous wall, here we investigate only the free space case (as in sections 3.1 and 3.2). In our FDTD simulations, we

used a high-fidelity Russian-made RPG-7 mesh, with a 2-mm resolution (figure 21). We considered that the entire assembly is made of metal (although some small parts are made of wood or ceramic materials, those are not important for the radar signature).

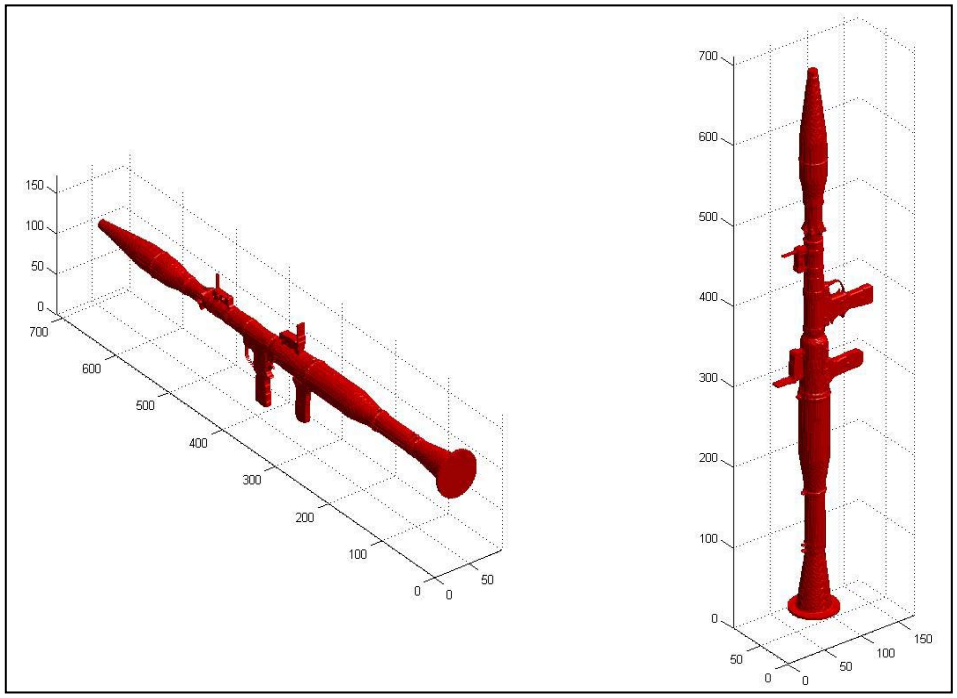

Figure 21. Different views of the RPG-7 mesh with 2-mm resolution (the tick marks on the axes represent numbers of FDTD cells).

In figure 22, we make an RCS comparison of a human alone versus a human carrying an RPG (similar to figure 7). We assume that the RPG is carried in an oblique position (45° tilt), as in figure 22a. The RCS values were computed in an angle interval of −30° to 30°, centered at broadside, and averaged over a 400-MHz frequency band centered at 1 GHz. Figure 22b shows the RCS for V-V polarization, figure 22c for V-H polarization, and figure 22d plots the ratio between the two polarizations. The conclusion is very similar to that in section 3.1, namely that the cross-polarization signature of the human is strongly enhanced by the presence of the weapon.

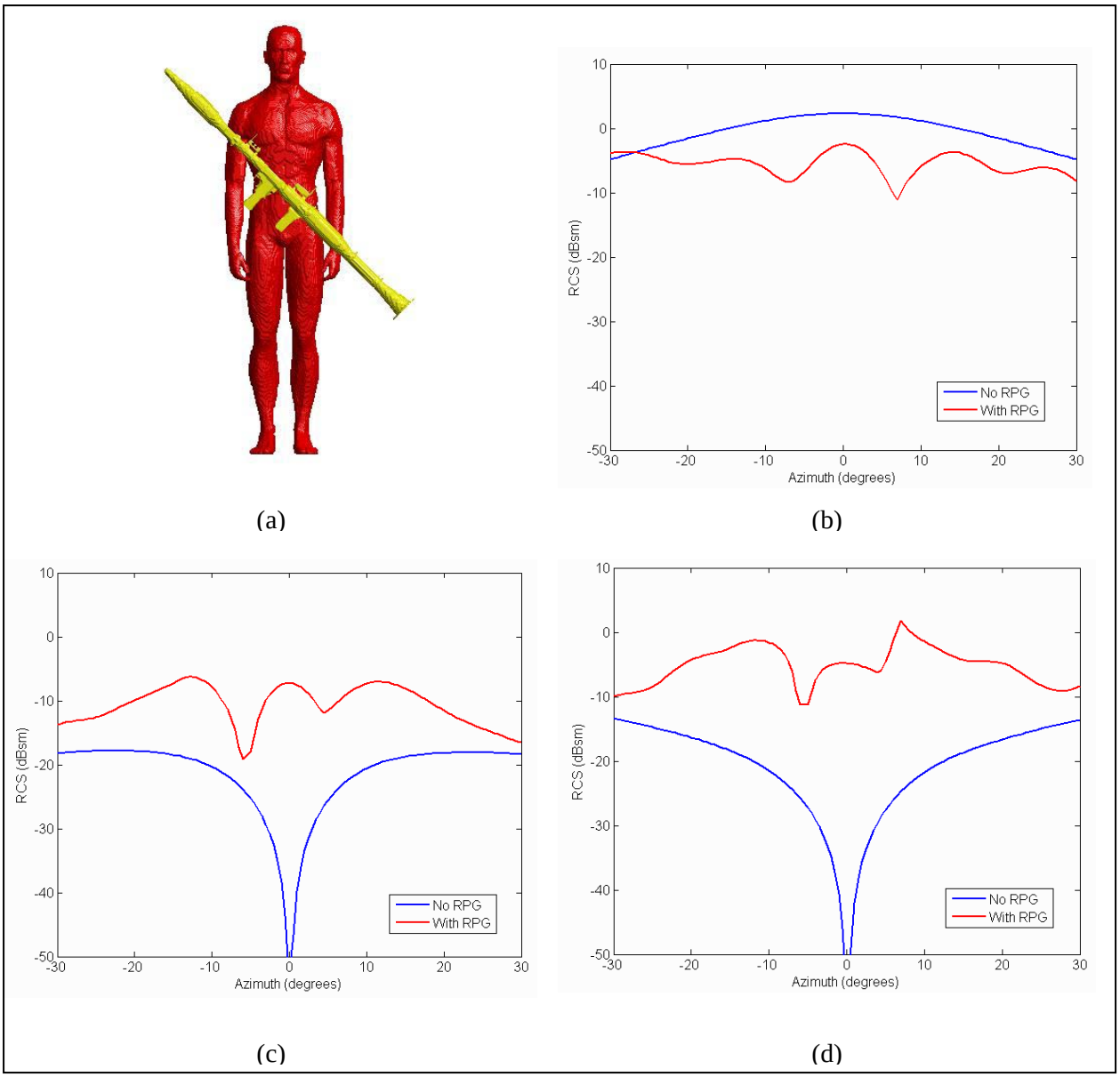

Figure 22. RCS of the standing human with and without an RPG versus azimuth angle showing: (a) the computational mesh; (b) RCS for V-V polarization; (c) RCS for V-H polarization; and (d) V-H to V-V RCS ratio.

Similar to section 3.2, we create SAR images of a human “carrying” the RPG in two positions, vertical and at 45° tilt. The images in figures 23 and 24 are based on the same algorithm and the same parameters as those in figures 8 and 9. One conclusion that we derive from figure 23b is that the V-V response of the RPG in vertical position is very strong, and it clearly enhances the V-V response of the human body (as opposed to the AK-47, which decreased the co-polarization response of the human body). This is made possible by the fact that the RPG has an RCS much larger than a rifle at broadside. Also, from figure 24b, we do not see a significant enhancement in the cross-polarization response of the human with the vertical RPG. In fact, the ratio of the brightest cross- to co-polarization pixels in the images is –27 dB, which is worse than the –23 dB in the case of the human body alone. Obviously, this metric cannot be used to discriminate a human carrying an RPG in vertical position. However, in this case the V-V polarization signature of the RPG becomes significantly larger than that of the human alone, so this signature alone can be used as a metric in discriminating the human carrying the weapon. Additionally, notice that the H-H image of the human with the vertical RPG (figure 23d) also shows a strong radar response for this polarization as well.

For the RPG tilted at 45°, the cross- to co-polarization ratio is –17 dB, which, although not as good as in the case of the AK-47, gives a 6 dB enhancement over the human body alone. In this case, the SAR images (both V-V and V-H) display a peculiar shape, caused by the significant cross-range extent of the RPG. This suggests that a detailed analysis of the image based on shape recognition can reveal the presence of the weapon more reliably than the polarimetric techniques introduced in this study.

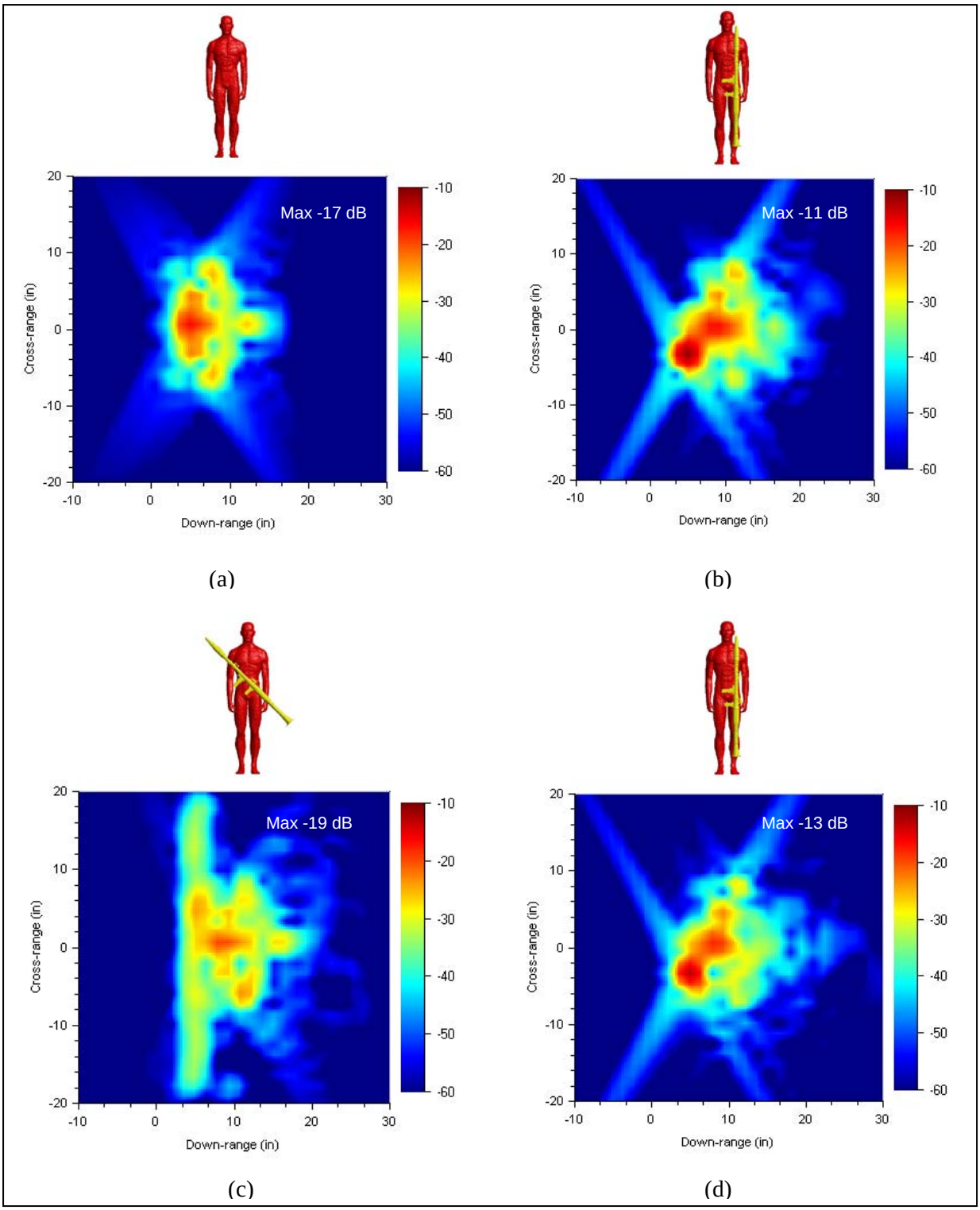

Figure 23. Co-polarization SAR images of a human with and without an RPG showing: (a) human without RPG, V-V polarization; (b) human with vertical RPG, V-V polarization; (c) human with RPG tilted at 45°, V-V polarization; and (d) human with vertical RPG, H-H polarization.

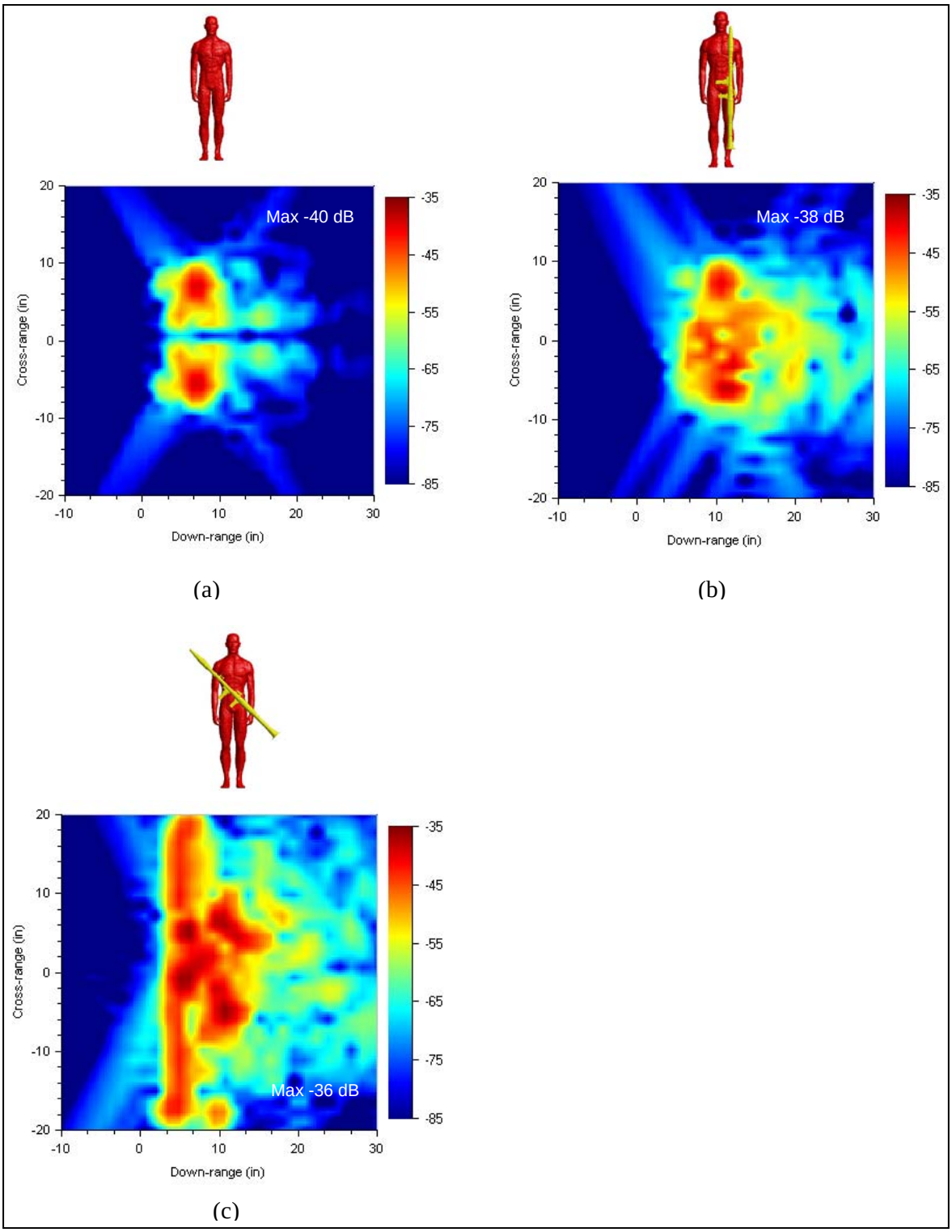

Figure 24. Cross-polarization (V-H) SAR images of a human with and without an RPG showing: (a) human without RPG; (b) human with vertical RPG; and (c) human with RPG tilted at 45°.

4. Conclusions

This study presented polarimetric radar approaches that could be used in detecting small weapons concealed behind walls. The techniques rely on the fact that the radar signature of targets with a large shape factor is strongly polarization-dependent. We exploited this property for weapons such as rifles (AK-47) or RPGs. The emphasis was on weapons carried by humans. In this context, the problem could be reformulated from detecting a weapon to discriminating a human carrying a weapon from a human without a weapon. It is important to emphasize that the approaches presented in this report do not apply to small weapons (such as handguns) that do not satisfy the large shape factor requirements. Also essential to our approach is that the weapons are passively carried by humans (as, for instance, in the port-arm position), such that the radar illuminates the target mostly at broadside. These techniques do not apply to a rifle or RPG held in the shooting position, where the radar illumination is straight along the barrel.

We first introduced a signature optimization procedure based on polarization direction transformations. Our computer models showed that this technique works as expected on an isolated rifle in free space, but breaks down in a more complex scenario where the rifle is carried by a human. A more robust approach is based on the strong cross-polarization response of a tilted rifle. In order to maximize the signature difference between a human carrying a weapon and a human without a weapon, we used the cross- to co-polarization return ratio. By simulating multiple STTW radar imaging scenarios, we demonstrated that this ratio is enhanced by at least 8 dB in the presence of an AK-47 rifle. The major advantage of using the ratio of two different signatures of the same target for discrimination is that this procedure is largely independent of target size (in other words, by scaling up the target dimensions we do not change the cross- to co-polarization ratio). We developed a weapon detection algorithm based on SAR images and successfully applied it to the simulated image of a complex room containing personnel with or without rifles. We also applied this idea to a Doppler radar scenario that looks at a walking human, where the discrimination is based on magnitude differences in the Doppler spectrum.

The through-the-wall imaging examples presented in this report included mostly homogeneous walls (although some included windows and doors). It is very possible that the additional amount of clutter introduced in an image by inhomogeneous walls (such as those built from cinder blocks) may degrade the discrimination potential of our approach. Another problem of great interest that we have not investigated here is searching for weapon caches hidden inside walls or other concealed building enclosures. We expect this application to benefit again from operating the radar in cross-polarization mode, since the walls mostly disappear from the images created in this mode.

It is important to mention that operating a through-the-wall imaging radar in cross-polarization could prove very challenging. One obvious issue is that the cross-polarization signature of targets

behind walls is usually very weak, especially after the radar waves incur a round-trip through the wall attenuation. In order to obtain signals above the noise floor in this mode, the radar design must include a low noise figure and a high dynamic range. Another difficult problem is the fact that typical wide-beam antennas (such as horn antennas), used in SAR systems at frequencies characteristic to STTW radar, do not display a pure polarization (either vertical or horizontal) away from boresight (*17*). That means it is impossible to obtain pure cross-polarization signatures of targets directly from radar measurements using these antennas (notice that this is not an issue for higher frequency SAR systems, where small integration angles about boresight are required, so the pure polarization assumption is mostly valid). A possible solution to this problem is to perform a polarimetric calibration of the radar by introducing a post-processing compensation procedure (*18*). Another possible approach would involve designing a wide-beam antenna with very low secondary polarization pattern at angles away from boresight.

Finally, we present a diagram (figure 25) meant to illustrate the benefits of using the cross-polarization mode in the wider context of STTW radar for military urban operations. We considered four types of targets that are frequently present in a STTW scenario: walls, furniture objects, humans and rifle-like weapons. The interest in detecting these targets usually increases from walls and furniture objects (which are considered clutter) to humans and eventually weapons carried by humans. As illustrated in figure 25, the cross-polarization signature of these targets also increases in the same order (from walls to weapons), whereas the co-polarization signature strengths follow the exactly opposite order. This suggests the use of the cross-polarization to co-polarization ratio as a good way to enhance the response from the most interesting targets (humans and weapons) while at the same time rejecting the clutter (walls and furniture in the scene). This metric can also be used as a discrimination tool in STTW imaging radar (as shown in sections 3.3 and 3.4) or Doppler radar (as shown in section 3.5). Although the operation of the radar in fully polarimetric mode presents a series of practical challenges, it would be very interesting to see our ideas (supported here by modeling results) confirmed by experimental data.

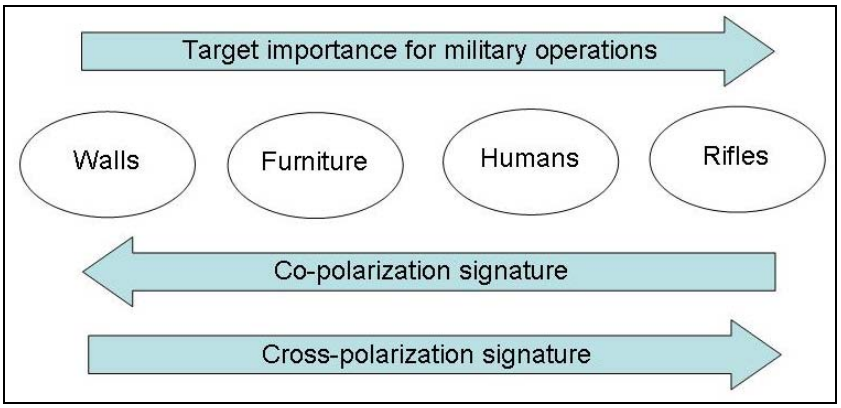

Figure 25. Diagram illustrating the typical STTW target hierarchy in terms of interest for military operations, together with the strengths of their co- and cross-polarization radar signatures.

5. References

1. Dogaru, T.; Nguyen, L.; Le, C. *Computer Models of the Human Body Signature for Sensing Through the Wall Radar Applications*; ARL-TR-4290; U.S. Army Research Laboratory: Adelphi, MD, September 2007.

2. Dogaru, T.; Le, C. SAR Images of Rooms and Buildings Based on FDTD Computer Models. *IEEE Transactions on Geoscience and Remote Sensing* **May 2009**, *47,* 1388–1401.

3. Dogaru, T.; Le, C. *Validation of Xpatch Computer Models for Human Body Radar Signature*; ARL-TR-4403; U.S. Army Research Laboratory: Adelphi, MD, March 2008.

4. Dogaru, T.; Le, C. *Simulated Radar Range Profiles of Simple Room as Computed by FDTD and Xpatch*; ARL-TR-4420; U.S. Army Research Laboratory: Adelphi, MD, April 2008.

5. Dogaru, T.; Le, C.; Kirose, G. *Time-Frequency Analysis of a Moving Human Doppler Signature*; ARL-TR-4728; U.S. Army Research Laboratory: Adelphi, MD, February 2009.

6. Agurto, A.; Li, Y.; Tian, G.; Bowring, N.; Lockwood, S. A Review of Concealed Weapon Detection and Research in Perspective. *Proceedings of the 2007 IEEE International Conference on Networking, Sensing and Control* **April 2007**, 443–448.

7. McMillan, R. W.; Currie, N. C.; Ferris, D. D.; Wicks, J. Concealed Weapon Detection Using Microwave and Millimeter Wave Sensors. *1998 International Conference on Microwave and Millimeter Wave Technology, Beijing, China,* 1998.

8. Federici, J.; Gary, D.; Barat, R.; Zimdars, D. THz Standoff Detection and Imaging of Explosives and Weapons. *Proceedings of SPIE* **2005**, *5781*, 75–84.

9. Farwell, M.; Ross, J.; Luttrell, R.; Cohen, D.; Chin, W.; Dogaru, T. Sense Through the Wall System Development and Design Considerations. *Journal of the Franklin Institute* **September 2008**, *345*, 570–591.

10. Taflove, A.; Hagness, S. C. *Computational Electrodynamics: The Finite-Difference Time-Domain*; Artech House: Boston, MA, 2000.

11. Ruch, G.; Barrick, D. E.; Stuart, W. D.; Krichbaum, C. K. *Radar Cross Section Handbook*; Plenum Press: New York, 1970.

12. Mott, H. *Remote Sensing with Polarimetric Radar*; Wiley-Interscience: Hoboken, NJ, 2007.

13. Carrara, W.; Goodman, R.; Majewski, R. *Spotlight Synthetic Aperture Radar – Signal Processing Algorithms*; Artech House: Boston, MA, 1995.

14. ARL MSRC Web page. http://www.arl.hpc.mil (accessed August 2007).

15. Gandhi, P. P.; Kassam, S. A. Analysis of CFAR Processors in Homogeneous Background. *IEEE Transactions on Aerospace and Electronic Systems* **July 1988**, *24* (4), 427–445.

16. Ranney, K.; Nguyen, L.; Ressler, M.; Stanton B.; Wong, D.; Koenig, F.; Tran, C.; Kirose, G.; Martone, A.; Smith, G.; Sichina, J.; Kappra, K. Change Detection Using the Synchronous Impulse Reconstruction (SIRE) Radar. *Proceedings of SPIE* **2008**, *6947*.

17. Balanis, C. *Antenna Analysis and Design*; Wiley: New York, 2002.

18. Barnes, R. M. *Polarimetric Calibration Using In-Scene Reflectors*; MIT Lincoln Laboratory Project Report TT-63: Lexington, MA, September 1986.

List of Symbols Abbreviations, and Acronyms

ARL	U.S. Army Research Laboratory
CAD	computer aided design
CERDEC	Communications-Electronics Research Development and Engineering Center
CFAR	constant false alarm rate
CPI	coherent processing interval
CPU	central processing unit
FDTD	Finite-Difference Time-Domain
EM	electromagnetic
H-H	horizontal-horizontal
I2WD	Intelligence and Information Warfare Directorate
I-Q	in-phase-quadrature
MSRC	Major Shared Resource Center
PDF	probability distribution function
RCS	radar cross section
RPG	rocket propelled grenade
SAR	synthetic aperture radar
STTW	sensing-through-the-wall
V-H	vertical-horizontal
V-V	vertical-vertical

No. of Copies	Organization
1 ELEC	ADMNSTR DEFNS TECHL INFO CTR ATTN DTIC OCP 8725 JOHN J KINGMAN RD STE 0944 FT BELVOIR VA 22060-6218
1	DARPA ATTN IXO S WELBY 3701 N FAIRFAX DR ARLINGTON VA 22203-1714
1 CD	OFC OF THE SECY OF DEFNS ATTN ODDRE (R&AT) THE PENTAGON WASHINGTON DC 20301-3080
1	US ARMY RSRCH DEV & ENGRG CMND ARMAMENT RSRCH DEV & ENGRG CTR ARMAMENT ENGRG & TECHNLGY CTR ATTN AMSRD AAR AEF T J MATTS BLDG 305 APG MD 21005
2	US ARMY RDECOM CERDEC I2WD ATTN AMSRD CER IW IM W CHIN (2 COPIES) BLDG 600 MCAFEE CENTER FT MONMOUTH NJ 07703
1	PM TIMS PROFILER (MMS P) AN/TMQ 52 ATTN B GRIFFIES BUILDING 563 FT MONMOUTH NJ 07703
1	US NAVAL RSRCH LAB RADAR DIV ADAPTIVE PROCESSING SECTION ATTN A DESROSIERS 4555 OVERLOOK AVE SW WASHINGTON DC 20375-5312
1	US ARMY INFO SYS ENGRG CMND ATTN AMSEL IE TD F JENIA FT HUACHUCA AZ 85613-5300
1	COMMANDER US ARMY RDECOM ATTN AMSRD AMR W C MCCORKLE 5400 FOWLER RD REDSTONE ARSENAL AL 35898-5000

No. of Copies	Organization
1	US ARMY RSRCH LAB ATTN RDRL CIM G TECHL LIB T LANDFRIED BLDG 4600 APG MD 21005-5066
1	US GOVERNMENT PRINT OFF DEPOSITORY RECEIVING SECTION ATTN MAIL STOP IDAD J TATE 732 NORTH CAPITOL ST NW WASHINGTON DC 20402
11	US ARMY RSRCH LAB ATTN RDRL CIM P TECHL PUB ATTN RDRL CIM L TECHL LIB ATTN RDRL SER M W O COBURN ATTN RDRL SER U A SULLIVAN ATTN RDRL SER U C LE ATTN RDRL SER U G KIROSE ATTN RDRL SER U K KAPPRA ATTN RDRL SER U M RESSLER ATTN RDRL SER U T DOGARU (2 COPIES) ATTN IMNE ALC HRR MAIL & RECORDS MGMT ADELPHI MD 20783-1197

TOTAL 23 (1 ELEC, 21 HCS, 1 CD)

INTENTIONALLY LEFT BLANK.